International Journal on Interactive Design and Manufacturing (IJIDeM) (2020) 14:631–650
https://doi.org/10.1007/s12008-020-00655-y

ORIGINAL PAPER

Albatros Create: an interactive and generative tool for the design and 3D modeling of wind turbines with wavy leading edge

Andrés Arias-Rosales[1] · **Gilberto Osorio-Gómez**[1]

Received: 24 February 2019 / Accepted: 9 January 2020 / Published online: 14 February 2020

Abstract
The shape of a wind turbine blade plays a critical role in the efficiency and robustness of energy production. In particular, the Wavy Leading Edge is a morphology that can be implemented in the blades to improve the operating range in unsteady conditions. The best performance is achieved by fine-tuning the blade geometry to the specific context. An aerodynamic exploration of these kinds of morphologies implies generating and evaluating design iterations. Accordingly, this work presents the development of the generative tool Albatros Create®. Through interactive visualization, infographics, and centralized parameterization, its goal is to support the geometrical definition of the aerodynamic surfaces of horizontal-axis turbines with or without a wavy leading edge. New airfoil profiles can be created, and 3D models of the rotors designed can be automatically generated. The software was implemented in the design of two rotors which were then recreated in a benchmarking analysis with four other softwares. None of the four managed to generate the smooth surfaces in fully-editable models that were achieved with Albatros Create. This work aims at empowering the research community with a user-friendly tool for exploring rotor designs through virtual prototypes. This can help to integrate further the design, modeling, and optimization stages, addressing a wider audience and facilitating the implementation of Wavy Leading Edge morphologies.

Keywords Wind turbines · Parametric CAD modeling · Wavy leading edge · Generative software · Design tool · Virtual prototype

1 Introduction and relevant literature

The efficiency of HAWTs (Horizontal-Axis Wind Turbines) is approaching its theoretical limit, with modern big-scale HAWTs exceeding 45% efficiencies [9]. However, such high performances are only sustained at steady nominal conditions regarding wind speed and direction, the turbulence level, and the optimal tip-speed ratio [26]. The performance tends to deteriorate whenever the wind conditions diverge from the ideal design scenario. These considerations are key for the energy production and cost-effectiveness of any wind project. Supporting the development of aerodynamic solutions that can extend the efficient operating range of HAWTs may favor a widespread adoption of wind energy.

✉ Andrés Arias-Rosales
aariasr@eafit.edu.co

Gilberto Osorio-Gómez
gosoriog@eafit.edu.co

[1] Design Engineering Research Group (GRID), Universidad EAFIT, Cra. 49 N. 7 Sur 50, Medellín, Colombia

One of the phenomena that may occur when wind settings are not nominal is a flow condition known as stall. It deteriorates the aerodynamic efficiency due to an increase in drag and an abrupt decrease in lift [26]. This condition is more likely to happen with high angles of attack [10], which may occur in HAWT blades when the tip-speed ratio is relatively low [32], such as when the rotor is starting to rotate, or when the angular velocity has not yet adapted to a gust [66].

The morphological feature known as Wavy Leading Edge (WLE) has been proposed as a passive flow control approach for delaying stall and improving the post-stall performance in turbomachinery [26,65]. This technology is inspired by the humpback whale's flippers, which have a wave-like leading edge with a series of protuberances [60]. This case of biomimicry is promising because the cross-section of their flippers is similar to wind turbine airfoils [26], and because the Reynolds conditions in both humpback whales and HAWTs are similar [14]. WLE may improve the operating range of wind turbines [14], and make the energy production more stable in highly unsteady conditions [66].

Nonetheless, different studies assessing this technology in turbomachinery present a range of positive, neutral or even negative aerodynamic effects. Favier et al. [21] observed a decrease in drag of up to 35%. Chen et al. [12] also found a decrease in drag but no significant effect on lift. Čarija et al. [11] found a delay in stall by 5°, a post-stall decrease in drag and increase in lift, but no considerable effects at pre-stall. Huang et al. [32] found that WLE can improve the efficiency at low tip-speed ratios, but deteriorate it at higher ranges. Similarly, Zhang and Wu [66] observed that WLE may improve or deteriorate the aerodynamic performance of a wind turbine depending on the tip-speed ratio. On the other hand, Asli et al. [4] observed an early stall, a lift reduction, and a drag increment, but the stall effect was smoother. The results vary with the level of complexity and the assumptions of the analysis. Notwithstanding, the general consensus suggests that WLE tends to delay stall, improve the post-stall efficiency, and may or may not deteriorate the pre-stall performance [65].

To achieve the full potential of this technology, the WLE parameters must be fine-tuned to the specific performance objectives, the blade baseline geometry, and the wind conditions [11]. However, the aerodynamic mechanisms by which WLE affects the performance are complex and three-dimensional [25,26], and there is not yet an analytical model that allows determining the best parameters directly. Thus, this fine-tuning implies an iterative process that needs to be further facilitated.

Generative tools can make iterative WLE explorations more accessible and effective. Generative tools are aimed at aiding in the definition of the proper geometry of a solution, in early design stages, with limited or preliminary input data [54]. Most reviewed studies do not specify the tools used for modeling the complex surfaces of blades with WLE. Huang et al. [32] developed their Computer-Aided Design (CAD) models with SOLIDWORKS®, while Čarija et al. [11] used CATIA®. However, such softwares with general CAD capabilities demand advanced surface modeling skills [6]. The users must parameterize the whole rotor and then translate this into modeling functions. This may be neither intuitive nor straightforward [64], especially if a WLE is introduced to the surface.

There are some softwares available with generative capabilities dedicated to wind turbine design. Falcon 3D Geodesign Tool allows iteratively testing new designs, but its generative capabilities are limited to the level of a wind farm instead of a turbine and its aerodynamic surfaces [51]. BOT is an Excel workbook for optimizing HAWT blade geometries [20], but its parameters [19] do not allow a controlled WLE exploration. Ashes [56,58] and Bladed [28] are HAWT design and analysis softwares. They both enable editing the blade geometry, but their visualization features and interactive functions are not focused on this aspect. JBLADE [44,55] and QBlade [40,41] (which integrates the wing and plane modeling software XFLR5 [18]) both provide generative modules that are focused on the blades' geometric exploration and provide interactive 3D visualization. QBlade has been used for different research projects to support the design, optimization and/or performance evaluation of HAWT rotors [3,38,43,46]. However, none of the available generative tools enables an intuitive, flexible, and centralized exploration of the WLE parameters.

The literature emphasizes the importance of developing generative tools for the design of HAWTs that are user-friendly [18,31,43,55,58], intuitive and accessible [31,41], visually rich [41,55,58], agile [51], and that can be used as teaching and self-learning tools [31,56,58]. Accordingly, this work presents the development of Albatros Create®, a novel generative and interactive tool. This software was developed in Microsoft Excel® with functionalities programmed in Visual Basic for Applications (VBA). Through geometric visualization and a mathematical control, its objective is to guide the definition of the parameters that determine the aerodynamic surfaces of HAWTs with or without a Wavy Leading Edge. An integration with SOLIDWORKS® allows the user to automatically obtain 3D CAD models from iterative designs.

Albatros Create is a user-centered tool developed within the Interactive Design framework. Interactive Design consists of supporting decision-making with modeling techniques dedicated to the real-time display and manipulation of cognitive, sensorial or physical interactions while exploring design solution spaces [23,24,47]. Interactive Design tools can allow a more flexible, efficient, and intuitive analysis and development of potential solutions by means of virtual representations and simulations. For instance, the work of Tzivelekis et al. [61] may facilitate the design of impeller-type geometries with an interactive application that automatically generates the 3D models. Similarly, seeking to make shoe design more effective and agile, Raffaeli and Germani [50] developed a CAD system for automating the most critical stages of shoes styling.

Albatros Create is an interactive tool in cognitive and sensorial terms because it allows the user to manipulate geometrical variables, it generates visual representations of the aerodynamic surfaces in response, and it provides interactive guidance for the user to define, explore, and navigate the geometry of a rotor solution. The resulting CAD models are exploratory virtual prototypes for the early design stages. The use of such early models has the potential to improve the effectiveness of new developments through quick and iterative visual and performance evaluations [37,64] that inform the successive more detailed stages. Designing and 3D modeling HAWT rotors implies manipulating mathematical models and employing sophisticated and time-consuming CAD techniques, especially if a WLE is implemented. Alba-

tros Create integrates this know-how intuitively. Thus, the contributions of this work seek to empower wind turbine innovation in industry and support engineers/designers in the research community with an accessible and effective tool for personalized HAWT designs. Moreover, this new tool can provide a hands-on educational and training experience, such as suggested in [42], for teaching about HAWTs in general.

This manuscript describes the conceptual structure of the software (Sect. 2), the variables and functions used to parameterize the aerodynamic surfaces (Sect. 3), the baseline optimization functionalities (Sect. 4), the graphical user interface (Sect. 5), the CAD modeling scheme (Sect. 6), and an implementation compared in a benchmarking analysis with similar tools (Sect. 7). For getting a grasp of how to use the tool, Sect. 2 locates the tool within the design framework, Sect. 5 provides a workflow that can be taken as the preferred method of use, and the implementation in Sect. 7 can serve as a valuable example. Albatros Create is openly available at a website of Universidad EAFIT [62].

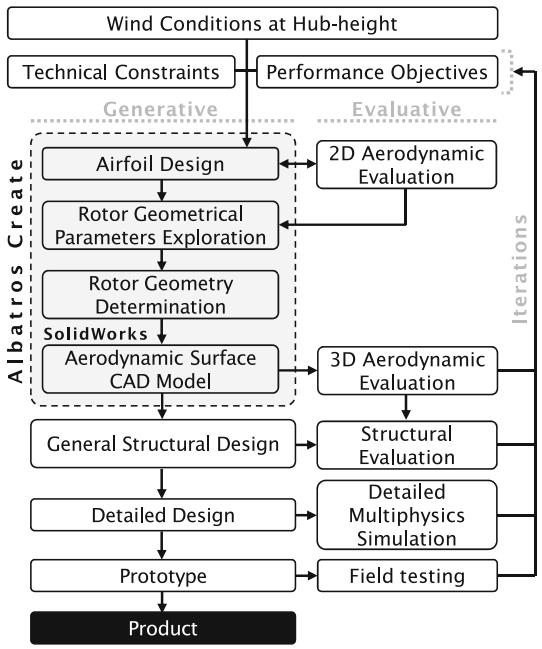

Fig. 1 Conceptual structure within the design framework

2 Conceptual structure in the design framework

Figure 1 presents the conceptual structure of Albatros Create, where its functionalities are contextualized and integrated within a design framework. Before iterating in a generative-evaluative design improvement process, the wind conditions, technical constraints, and performance objectives must be specified. As explained in Sect. 1, the best blade geometry, especially when WLE is implemented, depends on the specificities of the applied case. The wind conditions are usually characterized with the Weibull probability distribution [53], which has shape and scale parameters that can be fitted to locally measured data. Wind speed data is commonly measured at a standard height of 10 m above ground level [30]. Thus, to describe the conditions that a given wind turbine is expected to encounter, the Weibull parameters must be extrapolated to its hub-height [7,63]. These parameters can then be used for defining useful reference wind speeds, such as the mean, the most probable, and the one with maximum energy [22]. These speeds can be used for evaluating the aerodynamic performance at representative flow conditions.

The technical constraints must be identified, such as limits regarding size, weight, cost, or noise. The manufacturing processes may introduce constraints to the blade geometry, such as the minimum chord length and thickness of the blades, the tip shape and size, and the maximum surface curvature and its nature (e.g., concavity and convexity). It is also convenient to state the performance objectives for objectively choosing among the design iterations. These objectives may consist, for instance, in: satisfying a given energy or rated power need while minimizing costs or size; maximizing the energy or rated power while complying with the technical constraints; or maximizing the aerodynamic efficiency throughout the expected range of wind conditions.

Then, the generative design stage can be initiated with Albatros Create, which enables the design of airfoil sections, the interactive exploration of the rotor geometrical parameters, and the automatic modeling of the corresponding surfaces. For the rotor parameters exploration, it is convenient to first evaluate the 2D aerodynamic performance of the airfoils. This can be performed in parallel with other open and interactive softwares, such as QBlade [41] and XFLR5 [18]. The aerodynamic performance of the created CAD models can be assessed numerically with Computational Fluid Dynamics softwares, such as ANSYS® Fluent [5,11,66] or OpenFOAM® [14].

Figure 1 shows that the iterative process, where the results of the successive evaluations are compared with the constraints and objectives, can be performed at different stages, namely, after the aerodynamic design, structural design, detailed design regarding the different parts and subsystems, or with a physical prototype. The structural evaluation can be performed with finite element analysis softwares, such as the ANSYS® structural suite [13]. Also, tools like the SIMULIA Co-Simulation Engine [8] may be used for multiphysics detailed simulations.

Figure 2 presents the general structure of the modules and sub-modules of Albatros Create. The parameter exploration takes place in the Dashboard, at several levels of the rotor, and in the Airfoil Design module, at the level of NACA parameters [36]. The airfoils created or imported can be stored

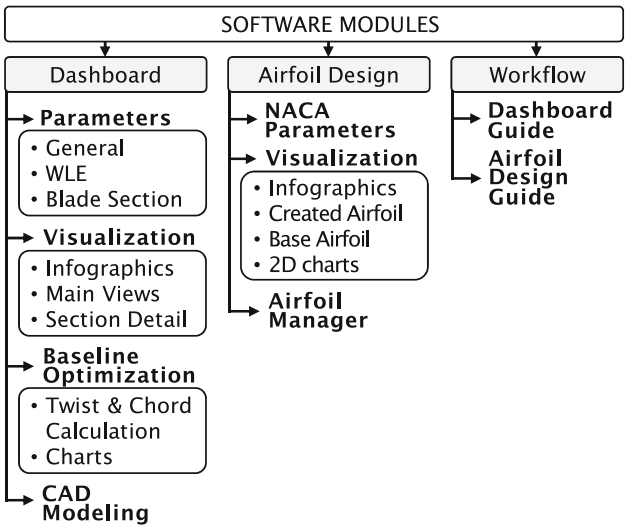

Fig. 2 Main modules and sub-modules of Albatros Create

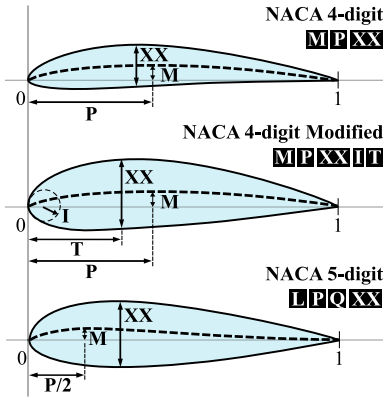

Fig. 3 NACA airfoils input parameters

and administered in the Airfoil Manager sub-module. In the Dashboard and Airfoil Design modules, interactive visualization features illustrate the general and detailed effects of the parametric exploration. Several infographics of the variables are available throughout the modules. Also, the Workflow module presents a scheme of the recommended method for using the other two modules. Furthermore, the Dashboard has sub-modules for optimizing the blade baseline geometry, and for directly exporting the rotor to the 3D modeling software SOLIDWORKS®.

3 Parameterization of the aerodynamic surface

This section presents the parameters and functions used in this work to define the aerodynamic surface of the rotor. The parameterization is determined at the level of the Airfoil curves; at the level of the blades, constituted by a series of cross-sections; and at the level of the rotor, constituted by the blades and the nacelle.

The blades can be described as a succession of aerodynamic cross-sections known as airfoils. Each section interacts with the relative local wind flow at 2D and 3D levels. The common practice is to first define the parameters from a 2D perspective, as illustrated in Fig. 3, and then consider the 3D flow implications in further iterations. For electrical power generation, the tip-speed-ratio (λ), namely, the ratio between the tangential speed of the tip of a blade and the actual speed of the wind, is usually $4 < \lambda < 10$ [39]. For such flow conditions, closed airfoils are preferred, as opposed to simpler curved plates [39]. Closed airfoils used in turbomachinery, and found in marine mammals, have a fusiform shape [26]. For lift-based wind turbines, such as HAWTs, the 2D objective of the airfoils is to maximize lift and minimize drag.

NACA airfoils [36] have a wide-spread use in turbomachinery because of their aerodynamic efficiency and versatility. Their contour is created by a set of equations that allow a flexible shape exploration through the manipulation of their input parameters. Albatros Create allows directly generating airfoils from several NACA families: 4-digit, 4-digit modified, and 5-digit. The digits refer to the input parameters, which are illustrated in Fig. 3.

M determines the maximum camber in the 4-digit and 4-digit modified. M is the height, in hundredths of the chord, measured from the chord line to the point where the central camber line has the largest curvature. P is the horizontal distance from the leading edge (the foremost edge) to the point where M takes place. It is measured in tenths of the chord and the input is halved in the case of the 5-digit. XX is the maximum thickness of the airfoil measured perpendicular to the chord line and in proportion of its magnitude. The 4-digit modified has an input T, in tenths of the chord, which determines the horizontal distance where XX takes place. This airfoil family also allows controlling the radius of a leading edge circle from an index I, which can be used to determine the leading edge sharpness. The 5-digit does not have a direct M input, but this parameter varies in proportion to an input L. L is related to the design *Lift Coefficient* (C_L), where $C_L = L\,(3/20)$. Lastly, Q determines whether the camber line is standard (Q = 0) or reflexed (Q = 1). A reflexed camber line curves upwards near the trailing edge (the rear edge). The inputs for these three airfoil families can be iteratively explored seeking a specific shape or a specific aerodynamic performance.

NACA equations [1,35] allow calculating the coordinates that delineate the airfoil's silhouette. These calculations start by defining a series of horizontal steps (X) along the chord line, which is initially defined from 0 to 1. Then, to establish the camber line coordinates, the corresponding vertical values are calculated. The airfoil thickness at every camber point

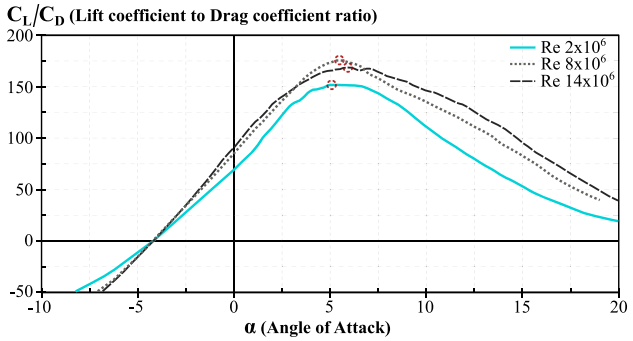

Fig. 4 Lift-to-drag ratio (optimal cases are circled) in function of the angle of attack for the NREL S818 airfoil

is calculated perpendicularly and symmetrically to the camber line. This results in the (X, Y) coordinates that delineate the upper and lower curves of the airfoil.

As it can be seen in Fig. 3, the region near the leading edge has a more pronounced curvature. Thus, it is convenient to have more (X, Y) resolution near this region. Accordingly, the horizontal camber coordinates (X_c) were defined by Eq. 1.

$$X_{ci} = \left(\frac{i-1}{N_{pc}-1}\right)^2 \tag{1}$$

where i is an integer ranging from 1 to the number of points in the camber line (N_{pc}).

There are other kinds of airfoils that may be used in wind turbines, such as the NACA 6-series [59], NACA 7-series [2], and the NREL families of airfoils [57]. Regardless of the airfoil shape, the lift and drag forces induced by it vary in function of the angle of attack. Figure 4 illustrates this with an NREL S818 Airfoil. Its 2D performance was evaluated with QBlade® for different Reynolds numbers. As part of the Airfoil parameters, the design *Angle of Attack* (α) is determined by these kinds of analyzes. The common practice is to calculate an expected range of Reynolds conditions for the particular application and then select the α that maximizes the lift-to-drag ratio (C_L/C_D) [39]. One important consideration is to choose an α which is not too close to the Stall region (see Sect. 1), which may abruptly deteriorate the aerodynamic performance with flow variations.

Figure 5 shows a general scheme of some of the main parameters at the level of the blade sections and the whole rotor. The rotor, with a Diameter D, is composed of N_B number of blades which are angularly equidistant. The *Nacelle Diameter* (D_N) determines where the blades start, namely the blade Roots. The Roots are circular sections with a diameter D_R. A blade's surface transitions from its Root to the airfoil sections, distributed with any radial distance (Z) between the nacelle radius $(D_N/2)$ and the rotor radius $(D/2)$.

The close-up in Fig. 5 shows how the airfoil chords tilt from the rotor plane with a *Twist Angle* (θ) seeking to maintain the design angle of attack (α) with respect to the local relative wind (W_R). As illustrated by the "Speed Triangle" (bottom-right corner), W_R results from the vector sum between the free wind reaching the rotor plane and the local tangential wind that results from the rotation at angular velocity ω. As shown, the free wind vector is reduced in magnitude according to the *Axial Induction Factor* (a), while the local tangential wind speed vector is increased according to the *Rotational Induction Factor* (a') [27,45]. The interaction between the vectors in the Speed Triangle also determines the local *Relative Flow Angle* (Φ). The farther a blade section is from the center of the rotor, the larger the local tangential wind speed, which increases the magnitude of W_R and reduces Φ. Therefore, to maintain the desired α along the blade, the sections must have an angular twist in θ.

A blade's surface will ultimately be determined by how the cross-sections are scaled, displaced, and tilted. These transformations also determine the shape of the leading edge and how the WLE is parameterized and controlled. Figure 6a illustrates how an airfoil can be scaled with the *Chord Length* (L_c), displaced parallel to the chord line with Δ_{par}, displaced perpendicular to the chord line with Δ_{per}, and tilted with θ. Figure 6b presents the main geometric layout used in this work for a HAWT blade with WLE. Gasch and Twele [27] state that "there is no recommendation in theory on how to arrange the individual blade elements along the radius with respect to the radial line". In the default layout, the sections are aligned at their leading edges. But other popular layouts may be implemented, such as aligning the sections at the 25–30% of the chord length, where the aggregated aerodynamic forces tend to act [27]. The blade layout in Albatros Create establishes 10 sections besides the Root. The capability of defining an arbitrary number of blade sections is being considered for future versions of the software.

The WLE extends the length of the peaks where the bumps are located by μ. μ is used both for displacing (parallel to the chord line) and scaling the sections where the WLE peaks are. As it is seen in Fig. 6b, the final chord length (L_{ct}) results from adding μ to the baseline chord length (L_c). The original airfoil's proportions are preserved, so the WLE does not deform the sections.

In Albatros Create, the WLE can be controlled in three ways (see Fig. 7): Constant, Linear, or Parabolic. With a centralized approach, these modalities determine how the μ values are defined along a given trajectory. These trajectories determine the amplitude of the bumps, while their wavelength is determined by the individual Z radial distances.

In the case of Constant WLE, all the bumps have an amplitude $\mu = A_W$. With Linear WLE, the μ values of the bumps depend on a straight line controlled by the amplitude of the first bump (A_W) and the WLE length (L_W). Defining the

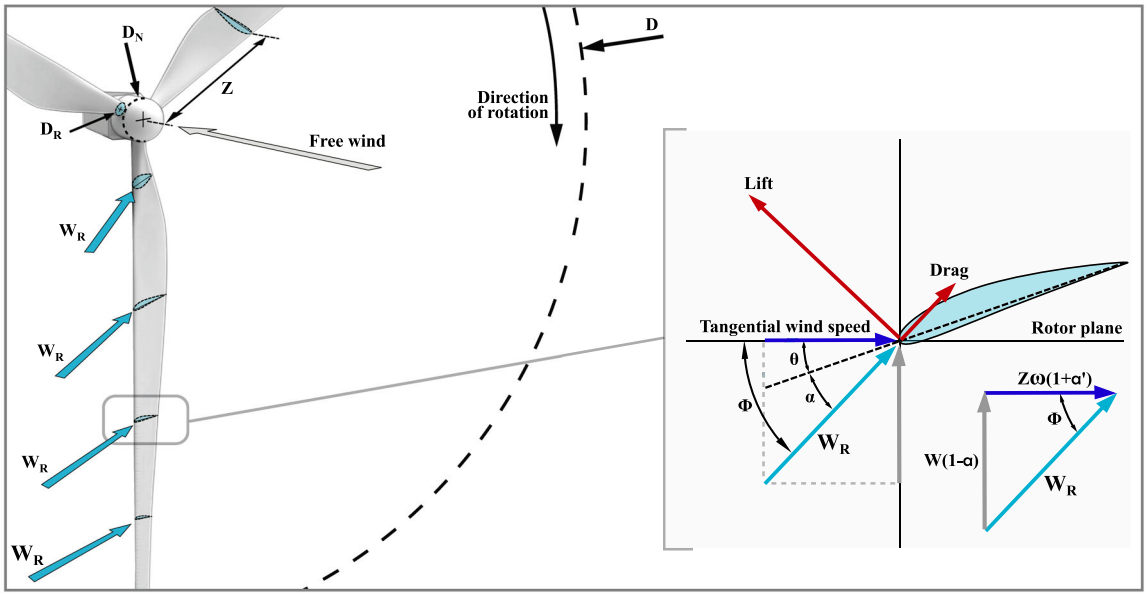

Fig. 5 Main rotor and blade parameters

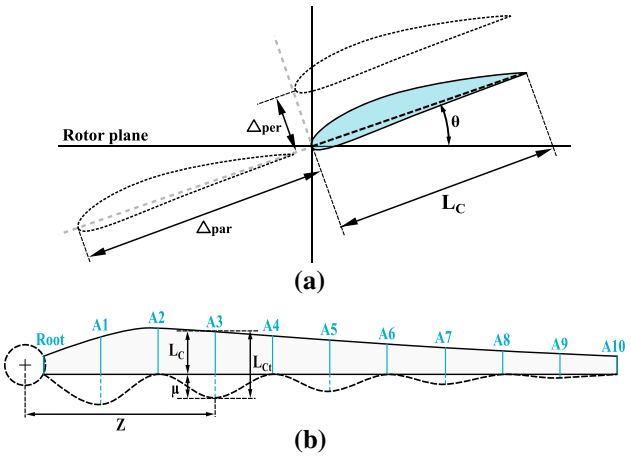

Fig. 6 Transformation parameters for determining the blade layout are shown in **(a)** and **(b)**. **(b)** is a flattened simplification where $\theta = 0°$ for all sections

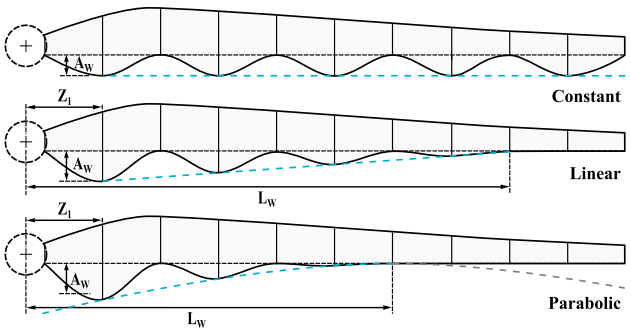

Fig. 7 Parameters controlling the wavy leading edge

straight leading edge of the baseline geometry as $Y = 0$, the equation of the straight line (Eq. 2) is fitted to the points (Z_1, A_W) and (L_W, 0). μ can be calculated with Eq. 3.

$$Y = mX + b \tag{2}$$

$$\mu = \begin{cases} \frac{A_W Z}{-L_W + Z_1} + \frac{A_W L_W}{L_W - Z_1}, & \text{if } L_W > Z \\ 0, & \text{if } L_W \leq Z \end{cases} \tag{3}$$

With Parabolic WLE, the μ values of the bumps depend on a parabolic curve, of the form Eq. 4, controlled by the amplitude of the first bump (A_W) and the WLE length (L_W). The vertex (h, k) of the parabola is set to the point (L_W, 0), and b is defined so as to fit the point (Z_1, A_W). μ can be calculated with Eq. 5. The parabola controlling the WLE is tangent to the straight baseline leading edge. Hence, this modality favors a smooth transition between the regions with and without WLE. L_W can be used to determine the number of bumps. For instance, the Linear modality in Fig. 7 has $L_W = Z_8$, so the number of bumps is limited to 4.

$$Y = b\,(X - h)^2 + k \tag{4}$$

$$\mu = \begin{cases} A_W \left(\frac{Z - L_W}{Z_1 - L_W}\right)^2, & \text{if } L_W > Z \\ 0, & \text{if } L_W \leq Z \end{cases} \tag{5}$$

Eqations 6–10 result in the transformed airfoil coordinates (X_3, Y_3). Both vertical and horizontal coordinates are first scaled by a factor ($L_c + \mu$). Then, the horizontal coordinates are displaced by ($\Delta_{par} - \mu$) and the vertical ones are displaced by Δ_{per}. The scaled and displaced coordinates (X_2, Y_2) are lastly tilted in Eqs. 8–10.

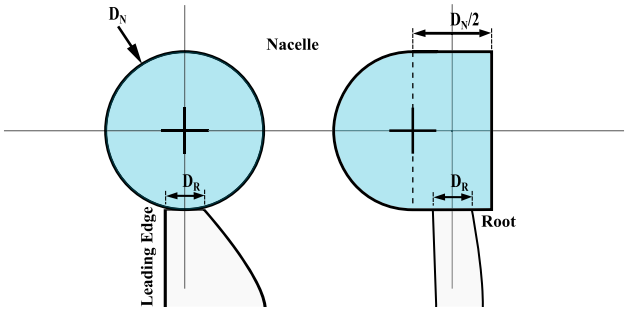

Fig. 8 Nacelle parameterization

$$X_2 = X_1\,(L_c + \mu) + \Delta_{par} - \mu \tag{6}$$

$$Y_2 = Y_1\,(L_c + \mu) + \Delta_{per} \tag{7}$$

$$X_3 = cos\,(\theta + \theta_0)\sqrt{(X_2)^2 + (Y_2)^2} \tag{8}$$

$$Y_3 = sin\,(\theta + \theta_0)\sqrt{(X_2)^2 + (Y_2)^2} \tag{9}$$

$$\theta_0 = \begin{cases} atan\,(Y_2/X_2)\,, & \text{if } X_2 > 0 \\ \pi + atan\,(Y_2/X_2)\,, & \text{if } X_2 < 0 \\ \pi/2, & \text{if } X_2 = 0 \text{ and } Y_2 > 0 \\ -\pi/2, & \text{if } X_2 = 0 \text{ and } Y_2 < 0 \end{cases} \tag{10}$$

These schemes and equations are related to a section view such as the one in Fig. 6a. This 2D view can be related to a 3D rotor, in terms of reference coordinates, by considering the blade in Fig. 6b with a clockwise 90° rotation. The 2D view would result from looking downward from the nacelle. This parameterization is related to a HAWT that rotates in the clockwise direction. For an anticlockwise rotating HAWT, the X coordinates must be inverted as $(X_3(-1), Y_3)$.

The nacelle was parameterized as simple as possible without additional geometrical inputs. The specific shape of the nacelle will depend on the mechanical transmission and electric generation subsystems within it. Here, the nacelle shape is designed generically for it to be modified by the users in further stages of the product development (see Fig. 1). As presented in Fig. 8, this shape is fully defined from D_N and symmetry alignments.

4 Optimization of the baseline geometry

A WLE implies complex 3D aerodynamic effects for which analytical models are not yet available (see Sect. 1,). Therefore, an iterative approach (see Fig. 1) is proposed. However, an optimized baseline (without WLE) geometry can be useful as a starting point before iteratively exploring the WLE. Depending on the aerodynamic considerations and simplifications, different models can be derived from the Blade Element Momentum theory (BEM) to determine this optimum baseline geometry. BEM is a well-known framework for calculating the aerodynamic forces in HAWT rotors [45]. It assumes an unchanging wind, no flow between blades, no radial flow between cross-sections, and no flexing of the blades. Albatros Create can also be used for the aerodynamic design of conventional HAWTs without WLE. In this case, the BEM-derived optimization models can be used to determine the sections' chord lengths and twist angles directly.

The Speed Triangle (see Fig. 5) shows that Φ can be calculated once the induction factors are known (a and a'). If the *Optimum Angle of Attack* (α_{opt}) has been identified as in Fig. 4, then the *Optimum Twist Angle* (θ_{opt}) is $\theta_{opt} = \Phi - \alpha_{opt}$. According to Betz [39], by assuming no drag, $a = 1/3$, and $a' = 0$ throughout the blade, θ_{opt} can be determined by Eq. 11

$$\theta_{opt} = atan\left(\frac{D}{3Z\lambda}\right) - \alpha_{opt} \tag{11}$$

Also ignoring the effects of drag, but considering the effects of rotation on the flow ($a' \neq 0$), Eq. 12 may be used for estimating θ_{opt} according to Schmitz [27,39].

$$\theta_{opt} = \frac{2}{3}atan\left(\frac{D}{2Z\lambda}\right) - \alpha_{opt} \tag{12}$$

On the other hand, the induction factors (a and a') can be directly calculated by iteratively solving the BEM equations with a given accuracy threshold [39,45]. This procedure is more realistic than the simpler assumptions of Betz and Schmitz, but it requires iterative numerical procedures that should be performed for every blade section in every blade design. Once a and a' are known, θ_{opt} can be estimated with Eq. 13 [27,39].

$$\theta_{opt} = atan\left(\frac{D\,(1-a)}{2Z\lambda\,(1+a')}\right) - \alpha_{opt} \tag{13}$$

Figure 9 illustrates how the twist angles vary along the blade with different optimization models. For this example, $\lambda = 5$ and $\alpha_{opt} = 6°$. The twist angles according to Betz and Schmitz start to converge here after 35% of the blade length. If Eq. 13 is calculated with $a = 1/3$ and $a' = 0$, the results are the same as the Betz simplification. Three other curves are shown with different induction factors to explore their effect on θ_{opt}. For more realistic results, the induction factors should be calculated for every blade section, but they are considered here as uniform throughout the blade for a simplified comparison.

Figure 9 shows that increasing a' results in smaller θ_{opt}. This is because, the larger a' is, the larger the local tangential wind speed vector in the Speed Triangle, which reduces Φ. Similarly, increasing a decreases θ_{opt} because the free wind vector becomes smaller in the Speed Triangle.

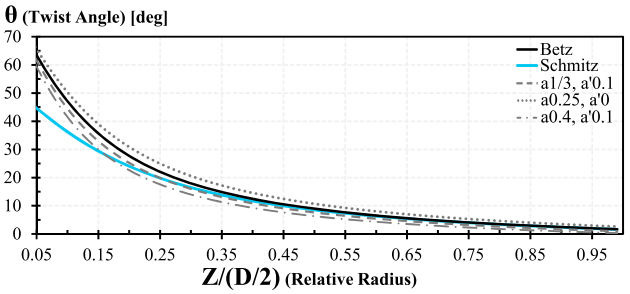

Fig. 9 Optimum twist angle according to several models

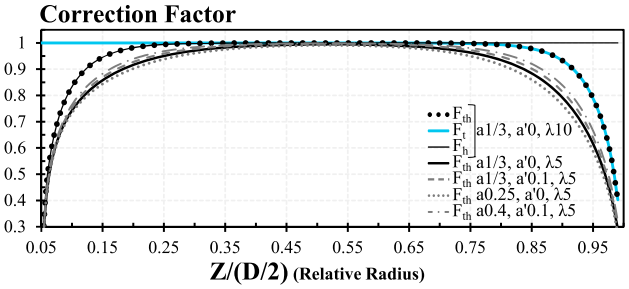

Fig. 10 Correction factor accounting for the induced vorticity near the edges of the blade

It is also possible to estimate *Optimal Chord Length* (L_{copt}) values from different assumptions and aerodynamic considerations. According to Betz [39], L_{copt} can be estimated with Eqs. 14–15, where C_L is the *Lift Coefficient* of a particular blade section measured at α_{opt}.

$$L_{copt} = \frac{4\pi D sin\Phi}{3N_B C_L \lambda} \tag{14}$$

$$\Phi = atan\left(\frac{D}{3Z\lambda}\right) \tag{15}$$

According to Schmitz's assumptions [27,39], Eqs. 16–17 may be used instead.

$$L_{copt} = \frac{8\pi Z\,(1 - cos\Phi)}{N_B C_L} \tag{16}$$

$$\Phi = \frac{2}{3} atan\left(\frac{D}{2Z\lambda}\right) \tag{17}$$

Following the same analysis shown for θ_{opt} in Eq. 13, if a and a' are known, Eqs. 18, 19 may be preferred as presented by El khchine and Sriti [20].

$$L_{copt} = \frac{4\pi a D sin\Phi}{N_B C_L \lambda\,(1 + a')} \tag{18}$$

$$\Phi = atan\left(\frac{D\,(1 - a)}{2Z\lambda\,(1 + a')}\right) \tag{19}$$

Some models allow complementing BEM with 3D corrections. For instance, the correction factor F_{th} described by Eqs. 20–24 accounts for the effects of the induced vorticity near the tips (F_t) and the hub (F_h) [45]. If one of these factors is not considered, it can be set to 1 in Eq. 24. For instance, if Winglet technology [33] is to be implemented, the effect of the induced vorticity near the tips is expected to be considerably reduced, so the correction factor becomes $F_{th} = F_h$.

$$F_t = \frac{2}{\pi} acos\left(e^{-f_t}\right) \tag{20}$$

$$f_t = N_B \frac{(D/2) - Z}{2Z sin\Phi} \tag{21}$$

$$F_h = \frac{2}{\pi} acos\left(e^{-f_h}\right) \tag{22}$$

$$f_h = N_B \frac{Z - (D_N/2)}{2Z sin\Phi} \tag{23}$$

$$F_{th} = F_t F_h \tag{24}$$

Figure 10 illustrates how the correction factor varies along the relative radius. The smaller the correction factor is, the more the performance is deteriorated by induced vorticity. For this example, $N_B = 3$, Φ is calculated with Eq. 19, and D_N is 5% of D. The first three curves show how F_{th} is composed by F_t and F_h. The fourth curve was calculated with the same induction factors but with a tip-speed-ratio $\lambda = 5$. Decreasing λ considerably deteriorates the aerodynamic performance at the inner and outer regions. The other curves are calculated with varying induction factors. Increasing a and a' increases F_{th} towards the edges.

Based on the work presented by Guo et al. [29], L_{copt} can be estimated with Eqs. 25 and 19 to account for the correction factor and the induction factors.

$$L_{copt} = \frac{8\pi Z a F_{th}\,(1 - a F_{th})\,sin^2\Phi}{N_B C_L\,(1 - a)^2\,cos\Phi} \tag{25}$$

Sedaghat et al. [52] go further in their considerations (Eq. 26) and also account for the *Drag Coefficient* (C_D) measured at α_{opt}.

$$L_{copt} = \frac{8\pi Z a F_{th} sin\Phi}{N_B C_L\,(1 - a)\,(cot\Phi + C_D/C_L)} \tag{26}$$

Figure 11 illustrates the effect of using the different L_{copt} models with the inputs: $N_B = 3, \lambda = 5, C_L = 1, C_D = 0.01$, $\alpha_{opt} = 6°$, $D_N = 5\%D$, $a = 1/3$, and $a' = 0.1$. Betz and Schmitz converge after 55% of the blade length. If a' were set to 0 for the other three models, they would follow the Betz curve and diverge only at the edges. A more realistic $a' = 0.1$ results in smaller relative L_{copt}. Similarly, Guo and Sedaghat follow the trajectory of the El khchine model in the

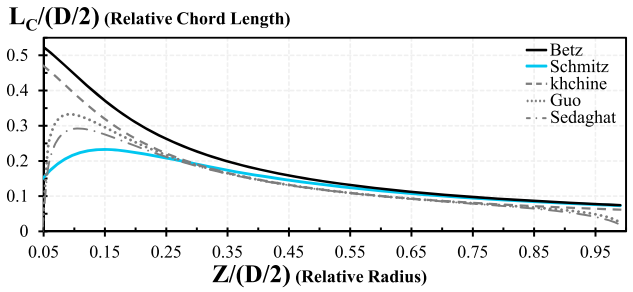

Fig. 11 Optimum chord length according to several models

central region but diverge towards the edges due to F_{th}. The Sedaghat model produces the smallest values and they would be even smaller with larger C_D values.

These models allow estimating the optimal chord lengths and twist angles for conventional HAWTs or as a baseline geometry for turbines with WLE. The users of Albatros Create may choose among them according to their assumptions and to the capacity of the users for calculating the inputs required. For instance, if there are no numerical tools available for estimating the induction factors, the Betz and Schmitz models may be used. Another approach is to perform exploratory CFD analyzes with geometries based on different models and choose the model that produces the best performance. Also, charts such as the ones in Figs. 9 and 11 may be compared with manufacturing constraints to select the most suitable geometry.

5 Graphical user interface and usability considerations

This section describes the GUI (Graphical User Interface) and its functionalities. Albatros Create is mainly based on a Microsoft Office Excel® workbook. The workbook has three main sheets visible to the users corresponding to the main modules: Dashboard, Airfoil Design, and Workflow. The most advanced functionalities, such as controlling SOLIDWORKS® for the CAD modeling, were programmed in Visual Basic for Applications (VBA). The software appears as an application that is dedicated only to the objectives of Albatros Create as opposed to a generic Excel workbook. All other conventional Excel functionalities are disabled or hidden.

Figure 12 presents the Dashboard GUI. The module is organized in interactive areas for entering the geometrical inputs, visualizing in real-time the changes in the blade geometry, and summarizing the blade parameters entered. After determining the General Inputs, the user can select each blade section and explore the transformation parameters shown in Fig. 6.

The WLE has a centralized control at the level of the blade, where the type of WLE is selected and then the corresponding parameters are defined as in Fig. 7. The changes in the blade geometry can be detailed in the Central and Orthogonal Views, where individual controls allow zooming and

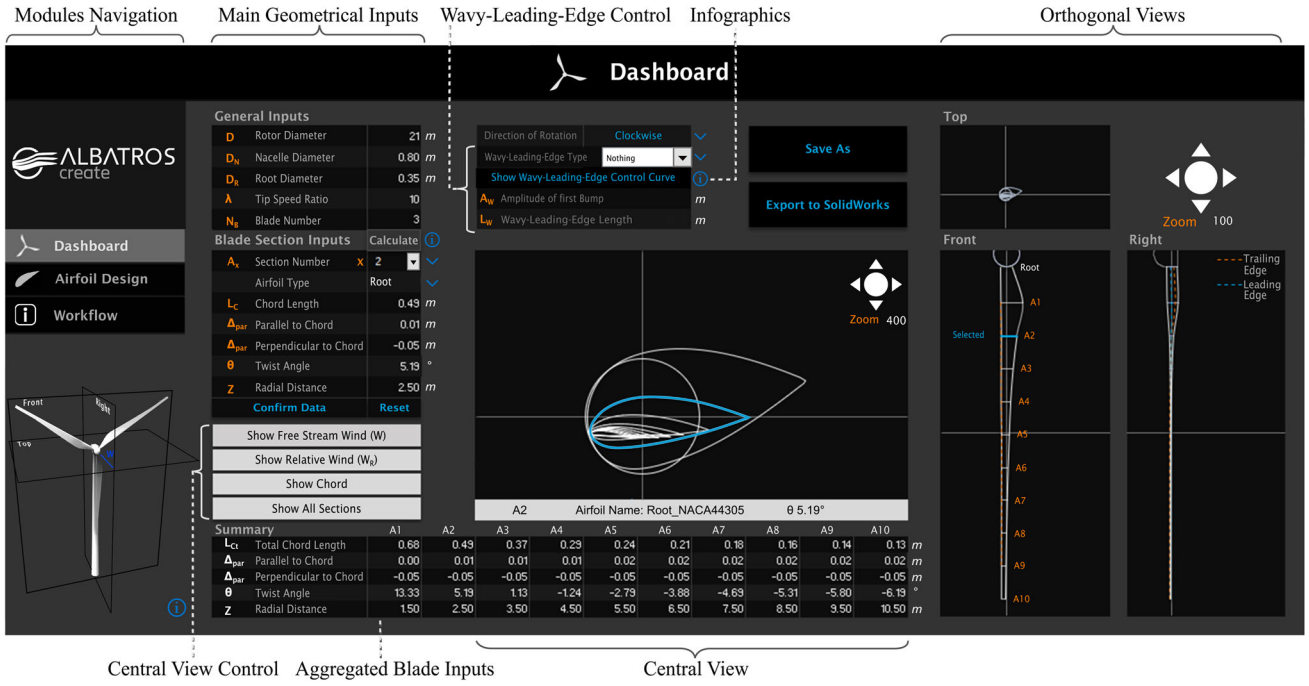

Fig. 12 Graphical user interface of the Dashboard module

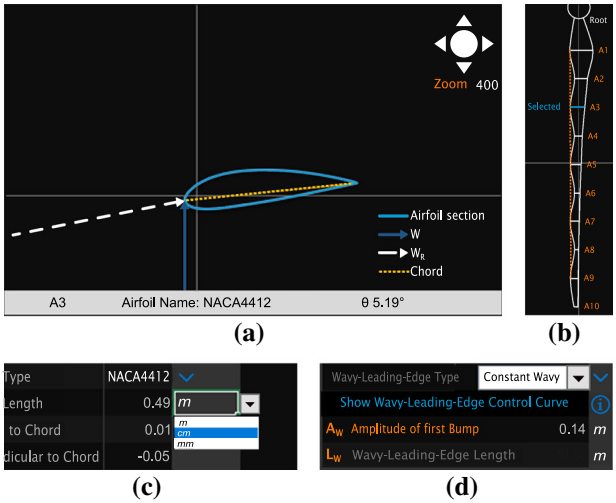

Fig. 13 Interactive features in the Dashboard

panning. The (i) icons provide infographics that explain the different parameters as in Figs. 5–7.

Figure 13 illustrates some of the interactive features in the Dashboard. When the "Show All Sections" button is disabled in the Central View Control, this view changes as in Fig. 13a. Here, the selected section can be detailed, including its interaction with the free wind (W) and relative wind (W_R) vectors. These vectors are calculated according to the Betz assumptions ($a = 1/3$ and $a' = 0$). Figure 13b shows how the Front view presents the WLE control curve. Also, as shown in Fig. 13d, the WLE controls activate the appropriate inputs according to the type of WLE selected. Other interactive features are the possibility to select the input units (see Fig. 13c) and a pop-up menu that allows scaling all geometrical parameters when D is modified. Similar interactive features can be found in the Airfoil Design module GUI (Fig. 14).

When the button Calculate is pressed (in the blade section inputs), the sub-module for baseline optimization pops-up as in Fig. 15. The user can select among the optimization models discussed in Sect. 4, enter the parameters indicated, and calculate the twist angle and chord length for a given section. This sub-module provides a visualization of the twist angles and chord lengths along the blade according to the various models (Fig. 15b). Here, the users can compare the results from the different optimization models with the actual values entered in the Dashboard. Also, these interactive charts can be used to visualize how the peaks in the WLE protrude from the baseline geometry.

Another important sub-module is the CAD Modeling pop-up, which appears with the "Export to SolidWorks" button in the Dashboard. Here, the user can check which CAD features are to be automatically modeled: the axis of rotation, the root extension of the blades towards the hub, the nacelle, and the airfoil chord lines. A VBA code opens SOLIDWORKS and starts modeling the rotor while the progress is announced in the sub-module.

Figure 14 presents the GUI of the Airfoil Design module. The user can select among NACA 4-digit, 4-digit modified, and 5-digit. For any given NACA inputs, the module shows the maximum thickness, the maximum camber, and the position of both as a proportion of the chord length. Once the user is satisfied with the airfoil shape, the coordinates can

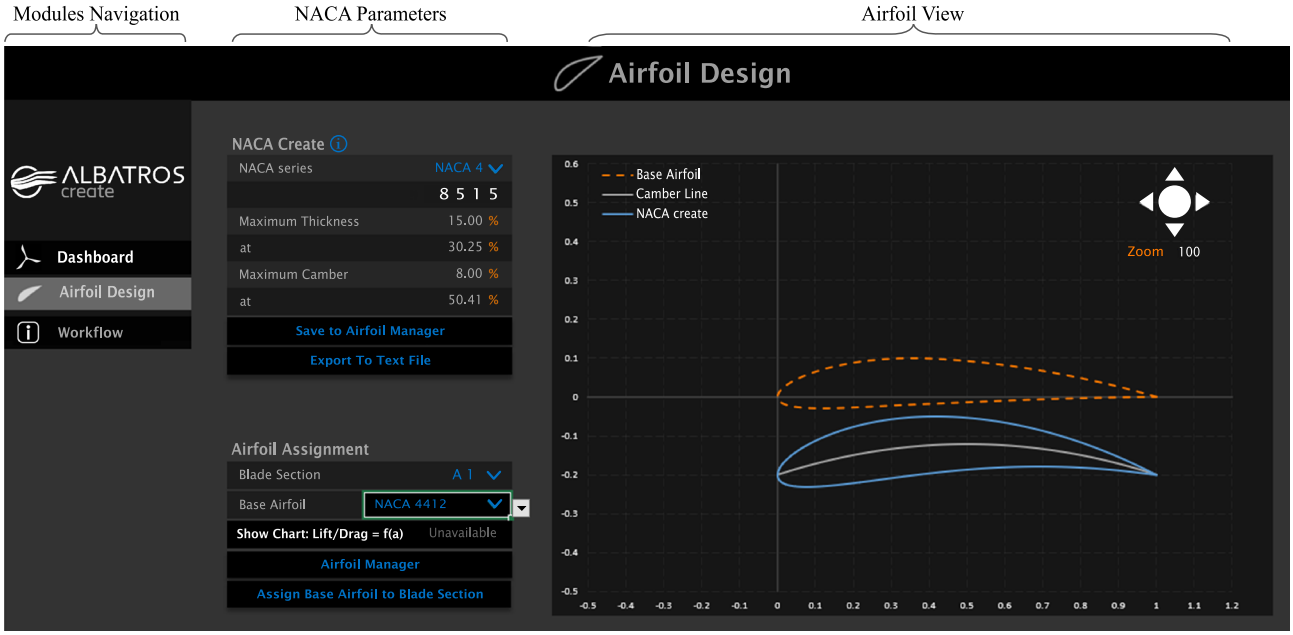

Fig. 14 Graphical User Interface of the Airfoil Design module

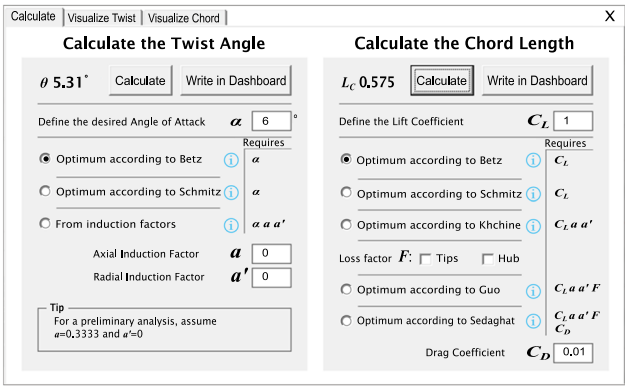

(a)

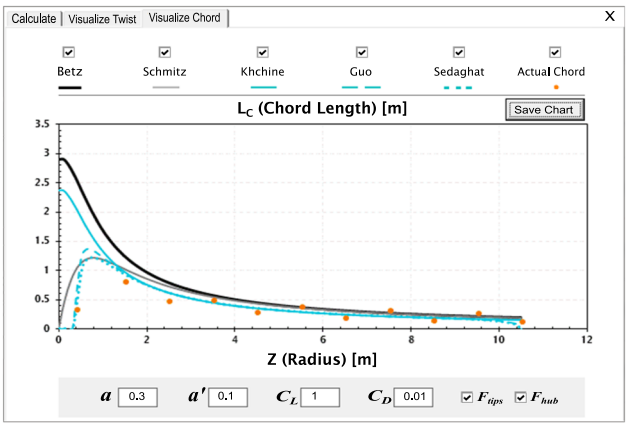

(b)

Fig. 15 Graphical User Interface of the Baseline Optimization submodule

be exported as a text file or saved to the Airfoil Manager database.

This module can be very useful for determining the shape of the sections near the root. As the root is circular, one or more intermediate sections are required for a smooth transition of the blade surface towards the airfoil-shaped cross-sections. The transition sections can be shaped in the Airfoil Design module as intermediates between a circle and the nearest airfoil shape.

Figures 16 and 17 present the schemes shown in the Workflow module. These workflows provide a detailed guide on the recommended use of the software. The information in Fig. 16 can be taken as the main generative method associated with the general functionalities of Albatros Create. Figure 17 presents the recommended method for specifically using the Airfoil Design module.

6 Automation of the CAD modeling

This section explains the general procedure with which Albatros Create generates 3D models by controlling the modeling capabilities of SOLIDWORKS.

From the parameters in the Dashboard, it is possible to determine the (X, Y, Z) coordinates of every blade section. X and Y come from the transformed (Eqs. 6–10) coordinates of the original airfoil profiles. The Z coordinates come from the radial distance of every blade section. What Albatros Create exports are points in space. The SOLIDWORKS "Curve Through XYZ Points" command is used to trace spline curves going smoothly through these points. Such a curve acts like a "default spline that is fully defined" [49], as with B-Splines [16].

These curves are traced in two directions, which allows the command "Boundary Boss/Base" [17] to generate the complex shape of a HAWT blade. Direction 1 is taken as the blade section closed curves. Direction 2 is characterized by the Leading and Trailing edges. However, if too many curves are selected for this modeling operation, the outer surface may get over-defined, resulting in unexpected behavior. For instance, the blade model shown in Fig. 18a was generated with eleven curves in Direction 1 (Root + 10 A sections) and 2 curves in Direction 2 (Leading and Trailing edges). With this set-up, it was not possible to generate a whole surface surrounding the body with a smooth curvature. Instead, two separate surfaces were generated and a sharp edge was observed in the Leading edge. The "Deviation Analysis tool" in SOLIDWORKS was used to calculate the angle between the surfaces at each side of this edge. When the surfaces are tangent, this angle is zero. Thus, the deviations shown in Fig. 18a reveal a discontinuous tangency. This discontinuity is also seen with the "Surface Curvature Combs tool". The first comb presents an overlap of the comb lines in the Leading edge. These comb lines also have a sudden change in length, implying an abrupt change in the curvature radius.

Seeking to improve the surface curvature quality, a blade shape was explored without including the Trailing edge as a curve in Direction 2. As shown in Fig. 18b, this improved the smoothness of the outer surface. No sharp edge is evidenced in the Leading edge. Moreover, the curvature combs show only smooth curvature variations. It appears that this less-restricted boundary shape adapts more naturally to the transitions required. Accordingly, this approach without the Trailing edge as a boundary curve is selected for the modeling algorithm.

VBA (Visual Basic for Applications) is used to automate the modeling functions of SOLIDWORKS based on its API (Application Programming Interface) [15]. The 3D modeling is performed with the steps described as follows and illustrated in Fig. 19.

1. The axis at the center of the rotor is modeled in the Y-axis with the "InsertAxis2" SOLIDWORKS API function.
2. A curve is modeled for every blade section, the Root, and the Leading Edge. This is performed through the "InsertCurveFilePoint" API function, which controls

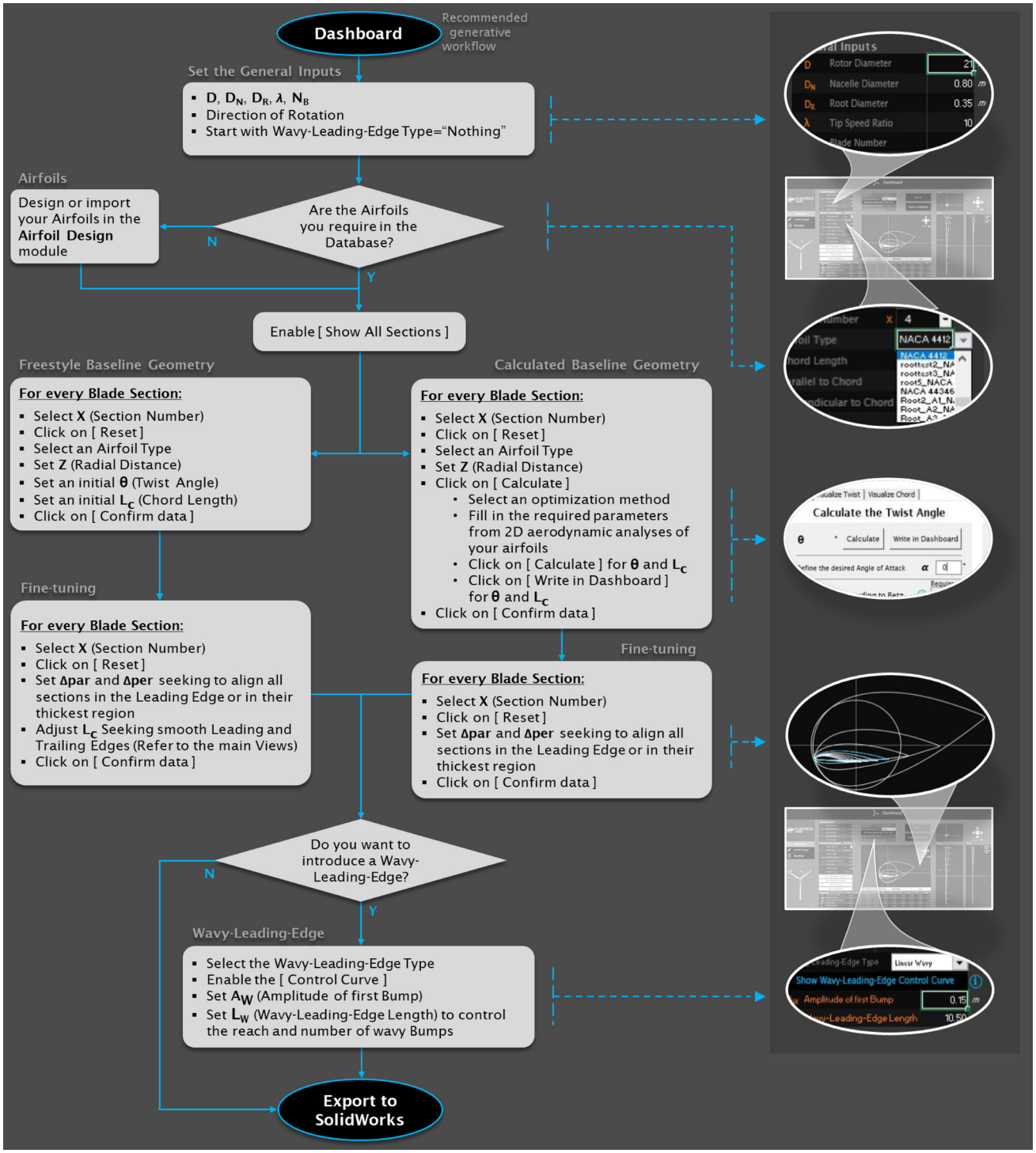

Fig. 16 Generative workflow of the Dashboard module

the SOLIDWORKS command "Curve Through XYZ Points".

3. The "InsertNetBlend" API function is used to generate a "Boundary Boss/Base" as the main body of one blade. It is created with the cross-sections in Direction 1, parallel to the XY plane, and the Leading Edge curve in Direction 2.
4. The "InsertSketch" API function is used to trace a circular sketch in the XY plane. This is a projection of the Root with diameter D_R.

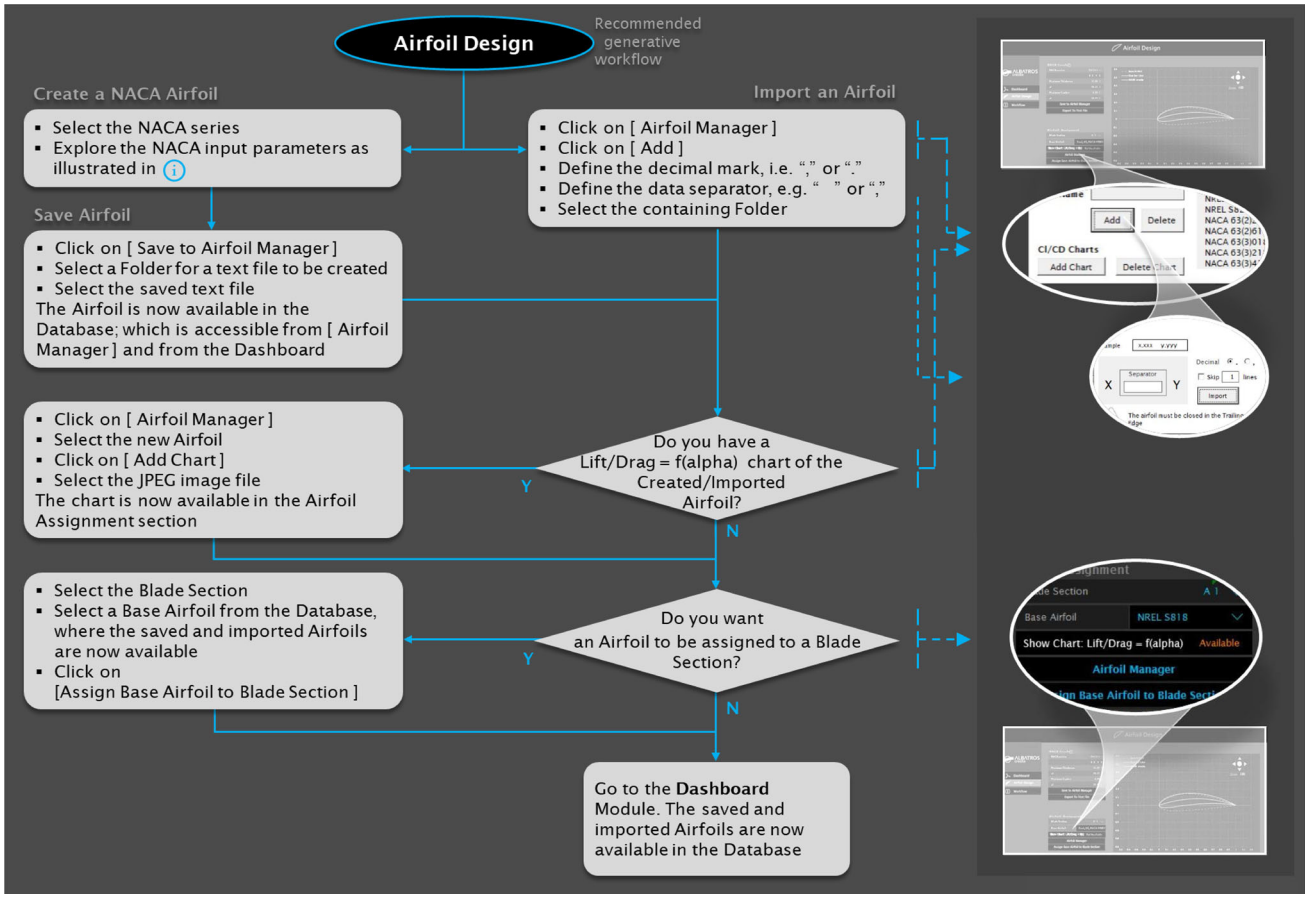

Fig. 17 Generative workflow of the Airfoil Design module

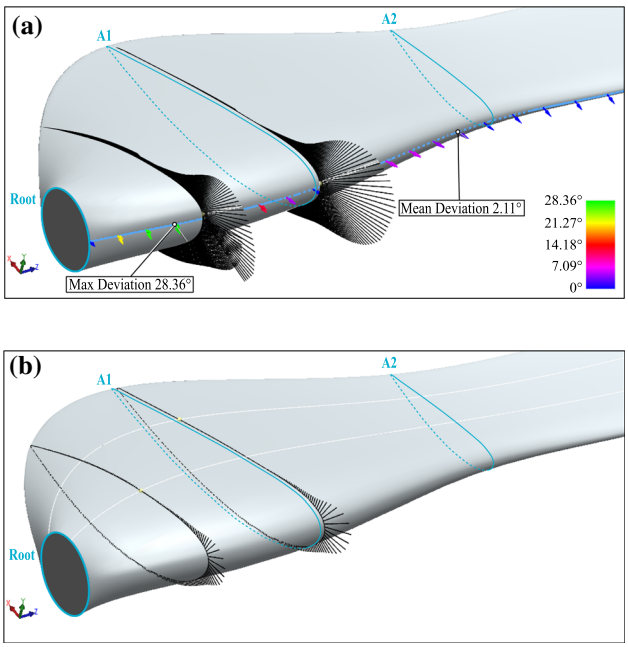

Fig. 18 Curvature exploration of a blade with WLE. The trailing edge is taken as a modeling input in **a**

5. The "FeatureExtrusion2" API function is used to extrude the sketch (Step 4) towards the Root section.
6. The "FeatureCircularPattern4" API function is used to perform a Circular Pattern of the blade and Root Extension bodies according to the number of blades (N_B).
7. With the same function and plane as in Step 4, half of the nacelle's shape is sketched as in Fig. 8.
8. The "FeatureRevolve2" API function is used to create the nacelle body by revolving the sketch of Step 7 around the axis of Step 1.
9. As in Step 2, the "InsertCurveFilePoint" API function is used to trace the Chord line of every blade section.

These steps automatically generate a solid body as parameterized in Albatros Create. All modeling operations appear in the Feature Manager Design Tree in SOLIDWORKS, where the users may inspect in detail how the model was created. The modeling process was designed to be easily editable and continued in further design stages. In particular, the chord lines traced in Step 9 provide useful reference points.

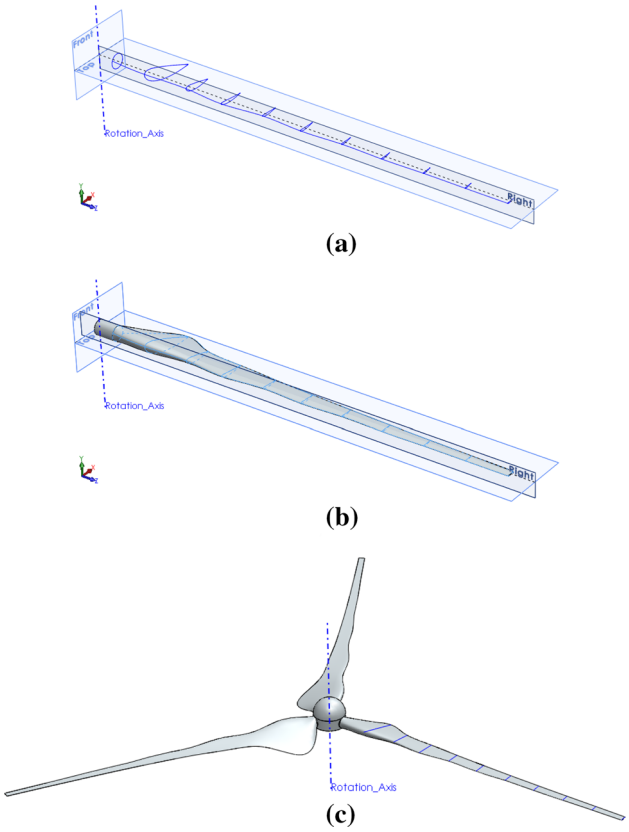

Fig. 19 3D modeling process in SOLIDWORKS controlled automatically from Albatros Create

7 Implementation and benchmarking

This section presents an implementation covering the generative steps related to Albatros Create and its control of SOLIDWORKS, and the evaluative step related to 2D aerodynamic analyzes (see Figs. 1, 16, and 17). The results are compared with similar implementations in other generative softwares.

First, the general inputs were determined in the Dashboard module with the values in Table 1. These inputs correspond to an initial baseline blade geometry without WLE.

Next, the NACA 4412 airfoil was selected for sections A3 to A10. As the initial root section is circular, sections A1 and A2 were used to make the transition smoother. Their shapes were determined by exploring NACA parameters in the Airfoil Design module and then inspecting the resulting blade shape in the Central View (Dashboard module). For this shape inspection to be effective, all sections should have initial L_c and θ values as close as possible to the final baseline geometry. Accordingly, the twist angles and chord lengths were defined for every section with the Schmitz optimization models (Baseline Optimization sub-module). As inputs for these models, $\alpha_{opt} = 10°$ and $C_L = 1$ were initially assumed. Then, Δ_{par} and Δ_{per} were fine-tuned to align the leading edges of all sections with the circumference of the Root section. From this exploration, A1 and A2 were defined as in Fig. 20. Both are NACA 4-digit modified, with the inputs 443053 and 442063, respectively.

Table 1 General inputs for the baseline blade geometry

D (m)	D_N (m)	D_R (m)	λ	N_B	Rotation	WLE
21	1	0.35	10	3	Clockwise	Nothing

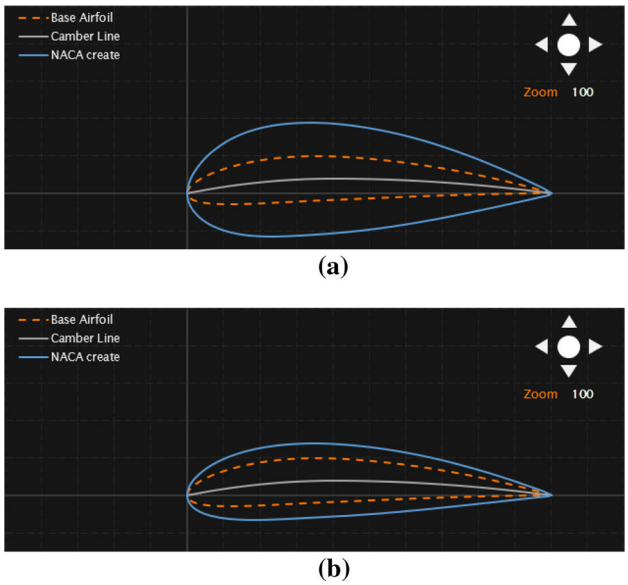

Fig. 20 NACA 4-digit modified airfoils for the sections **a** A1 and **b** A2, with NACA 4412 as the base airfoil

The next step was to improve the twist angles with more realistic α_{opt} values for the Schmitz models. As indicated in Fig. 1, 2D aerodynamic analyzes can be used to find α_{opt} considering the shape and Reynolds number (Re) of every section. Re (Eq. 27) considers the local velocity of the fluid, in this case W_R; a characteristic length, in this case L_c; and the kinematic viscosity (ν). By assuming $a = 1/3$ and $a' = 0$, W_R can be estimated with Eq. 28. ν was approximated as $1.46\text{E}{-5}\,\text{m}^2/\text{s}$ [48], and the free-wind speed was taken as $W = 10\,\text{m/s}$.

$$Re = \frac{W_R L_c}{\nu} \tag{27}$$

$$W_R = 2W\sqrt{\frac{\lambda^2 Z^2}{D^2} + \frac{1}{9}} \tag{28}$$

The 2D aerodynamic performance was assessed in QBlade (see Fig. 21), which requires the coordinates of a given airfoil, Re, and the Mach number. Mach is W_R divided by 343 m/s, the speed of sound [34]. This analysis allowed identifying the α_{opt}.

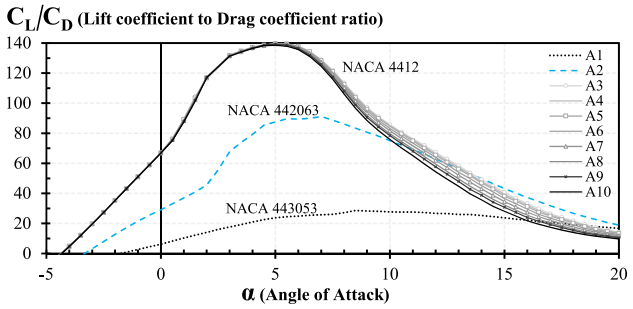

Fig. 21 2D aerodynamic analysis in QBlade of the blade sections

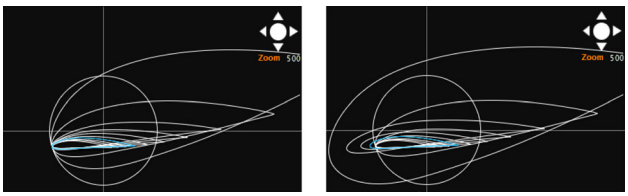

Fig. 22 Cross-sectional geometry of **a** the baseline blade and **b** the WLE blade

After re-calculating the twist angles, a final fine-tuning was undertaken through Δ_{par} and Δ_{per}. The resulting Baseline Blade is shown in Fig. 22a. Another version of the blade with WLE (The WLE Blade) was generated by changing the Wavy Leading Edge Type to Parabolic, setting the Amplitude of the first bump to $A_W = 15\%L_{c1}$, and the length to $L_W = D/2$. The cross-sectional effect of adding this WLE is illustrated in Fig. 22b.

Table 2 presents the parameters of the A1-A10 sections, as well as the results of the W_R, Re, Mach, and α_{opt} calculations. The L_c row corresponds to the chord lengths of the Baseline Blade, while the L_{ct} row corresponds to the WLE Blade.

With the CAD Modeling sub-module, both blade geometries were automatically generated in SOLIDWORKS. The corresponding renderings in Fig. 23 represent the final result of the Albatros Create generative process. These models achieved consistent surfaces with smooth transitions. Figure 24 presents an inspection of the smoothness of these surfaces through "zebra stripes". This tool allows assessing the curvature continuity. Abrupt changes in the surface would presumably be detectable through discontinuities in the stripes. No discontinuity seems evident. Moreover, a color code characterizes the surface regions according to their radius of curvature: The regions tending towards black are almost flat, whereas the ones tending to green present pronounced curvatures. As expected, the greener regions correspond to the Leading and Trailing edges.

The generative capabilities of Albatros Create were benchmarked against other relevant softwares. The same Baseline and WLE Blade geometries were attempted to be recreated with QBlade®, JBLADE®, Bladed®, and Ashes®.

In QBlade, airfoils can be created with a Spline free-form tool or with a NACA generator for only the 4-digit and 5-digit types. The blade geometry is determined by: number of sections, radial position, chord length, twist angle, offset displacement in the X and Y directions (according to the coordinates in this work), and a displacement analogous to Δ_{par}. Apparently, the direction of rotation cannot be changed. There are optimization functionalities but only according to Betz and Schmitz. A WLE can be introduced by manually scaling and displacing the sections corresponding to the peaks. However, an additional spreadsheet is needed to calculate how to adjust the sections as in Fig. 7.

QBlade has a 3D visualizer of the blades, which illustrates in real-time the changes in the geometry. It is engaging, but the lack of orthogonal views makes it challenging to fine-tune and understand the variations during a detailed exploration. Furthermore, the longitudinal transitions between blade sections are generated in straight segments. Thus, the surface may not be smooth and can present abrupt changes after every section. This can be evidenced in Fig. 25, which presents both

Table 2 Parameters of the A1-A10 blade sections, including the W_R, Re, Mach, and α_{opt} calculations

	A1	A2	A3	A4	A5	A6	A7	A8	A9	A10
NACA	443053	442063	4412	4412	4412	4412	4412	4412	4412	4412
W_R(m/s)	15.7647	24.7252	33.9935	43.3726	52.8035	62.2627	71.7390	81.2264	90.7215	100.2220
Re	1.109E6	1.239E6	1.285E6	1.305E6	1.316E6	1.322E6	1.326E6	1.329E6	1.339E6	1.332E6
Mach	0.0460	0.0721	0.0991	0.1265	0.1539	0.1815	0.2092	0.2368	0.2645	0.2922
α_{opt}(deg)	8.5	7.0	5.5	5.0	5.0	5.0	5.0	5.0	5.0	5.0
L_c (m)	1.0273	0.7316	0.5518	0.4394	0.3639	0.3101	0.2700	0.2389	0.2155	0.1941
L_{ct} (m)	1.1813	0.7316	0.6449	0.4394	0.4114	0.3101	0.2871	0.2389	0.2174	0.1941
Δ_{par} (m)	−0.0050	0.0000	0.0025	0.0050	0.0060	0.0070	0.0070	0.0085	0.0090	0.0095
Δ_{per} (m)	−0.05	−0.05	−0.05	−0.05	−0.05	−0.05	−0.05	−0.05	−0.05	−0.05
θ(deg)	14.8280	8.1883	5.6328	3.7560	2.2055	1.1175	0.3131	-0.3053	-0.7953	-1.1929
Z (m)	1.5	2.5	3.5	4.5	5.5	6.5	7.5	8.5	9.5	10.5

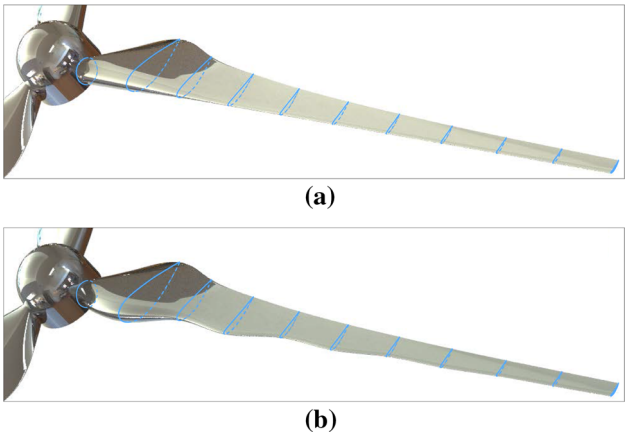

Fig. 23 Renderings of the CAD models corresponding to **a** the baseline blade and **b** the WLE blade

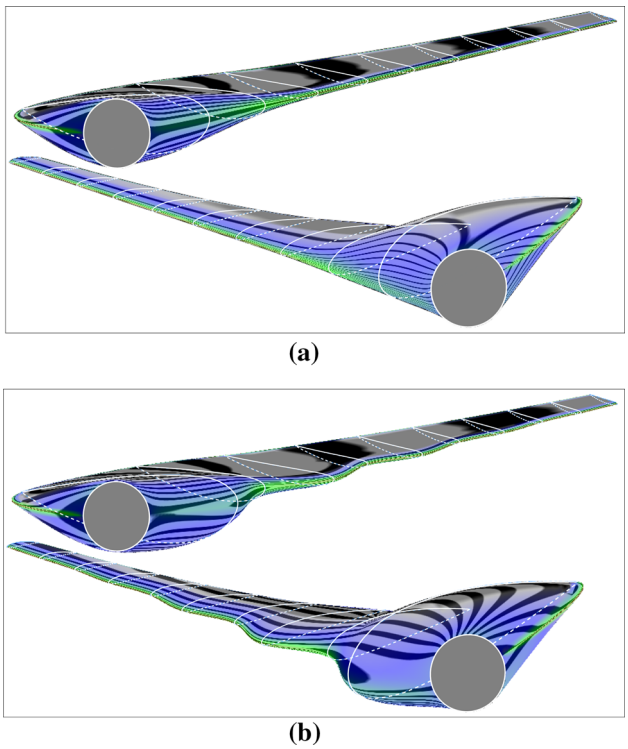

Fig. 24 Curvature analysis of the CAD models for **a** the baseline blade and **b** the WLE blade

blade geometries recreated in QBlade. The WLE results as a series of sharp peaks instead of the sought smooth surface.

QBlade allows exporting a blade as an STL file with a given resolution regarding the number of cross-sectional and longitudinal points; 20 and 200 as default, respectively. The STL blade geometries were imported in SOLIDWORKS as solids. Some errors were detected concerning normal faces but the software managed to generate the solid bodies. However, as presented in Fig. 25, these bodies do not have smooth surfaces because they are composed of flat triangles. Although the generated solid can be affected by other

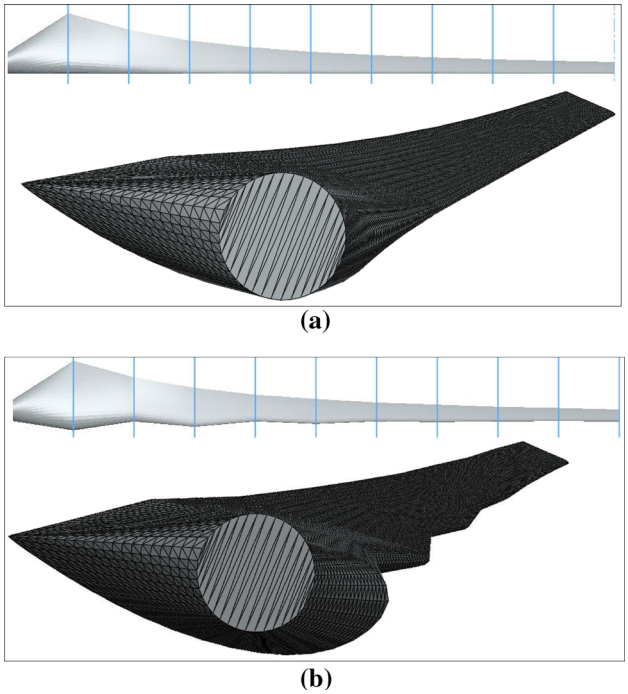

Fig. 25 Blade geometries recreated in QBlade® shown as visualized in QBlade (upper part) and as imported in SOLIDWORKS. **a** Baseline blade and **b** WLE blade

modeling features (e.g., cut extrusions), the feature that generated the solid in the first place cannot be edited. This is different from Albatros Create, where the modeling features can be edited by the user. Moreover, QBlade only exports one blade and not a whole rotor.

The blade geometries were also recreated with JBLADE. Although this is a propeller design tool, it can also be used for HAWT blades, so it is relevant for this benchmarking. In terms of airfoil design and management, JBLADE has almost the same functionalities and GUI as QBlade. However, it does not seem to be possible to include circular sections in the blade. Thus, the root sections had to be assigned the same airfoil type as A1 (see Fig. 26).

The generative module for exploring the blade geometry is very similar to QBlade in terms of the GUI, 3D visualizer, and geometrical parameters, but no optimization functionalities are available. The parameter "Dihedral" allows bending the blade around axes parallel to the X-axis (in the coordinates of this work). JBLADE also allows exporting the blade in an STL format, but without adjustable resolution. Thus, as can be seen in Fig. 26, the triangular faces are much larger, with each triangle extending from one blade section to the next one. When the geometries were imported from SOLIDWORKS, a series of issues with triangular faces were detected and only a surface was obtained instead of a solid body. Furthermore, some faces in the leading edge were lost in the process, which is highlighted in Fig. 26.

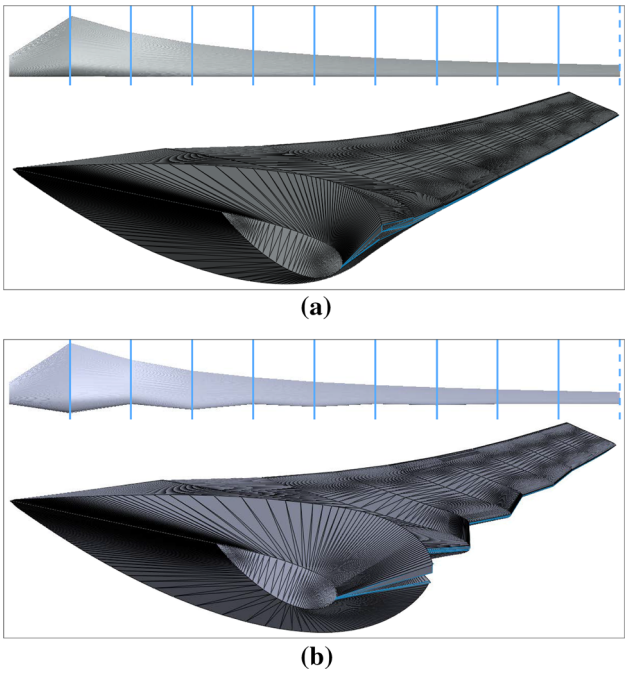

Fig. 26 Blade geometries recreated in JBLADE® shown as visualized in JBLADE (upper part) and as imported in SOLIDWORKS. **a** Baseline blade and **b** WLE blade

In the case of Bladed, it seems to be more focused on its evaluative capabilities than on supporting a generative exploration. The airfoil tools are very limited. The section profiles are generic airfoils that change their shape according to a thickness parameter. Therefore, it was not possible to recreate the airfoil types described in Table 2. Instead, the thickness parameter was used to emulate the maximum thickness of the target profiles. The circular root section was achieved by setting the thickness to 100% (see Fig. 27). Every section can be modified in terms of the chord length, twist angle, X and Y displacement, and parameters similar to Δ_{par} and Δ_{per}. Also, the direction of rotation can be determined, and there are parameters related to the shape of the tower and the nacelle.

Bladed presents blade geometry visualization features that are similar to features in the Dashboard of Albatros Create, such as the Central View, Front view, and the twist and chord length distributions in the Optimization module. However, these views do not allow zooming or panning, which makes it challenging to inspect details. Nor is there a view showing all the sections from a cross-sectional perspective (Fig. 22), which was of great use for fine-tuning in the implementation case. There is a 3D visualization tool, but it does not change in real-time during the geometric exploration. Both blade geometries were recreated as much as possible as seen in Fig. 27. The blade is defined with longitudinal straight segments, resulting in sharp WLE bumps. Furthermore, there is no clear tool for directly exporting the blade or rotor geometry in a file format that is compatible with CAD softwares.

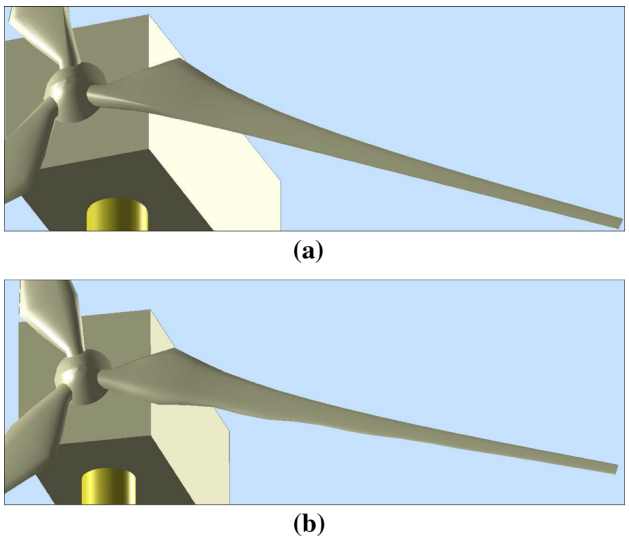

Fig. 27 Blade geometries recreated and visualized in Bladed®. **a** Baseline blade and **b** WLE blade

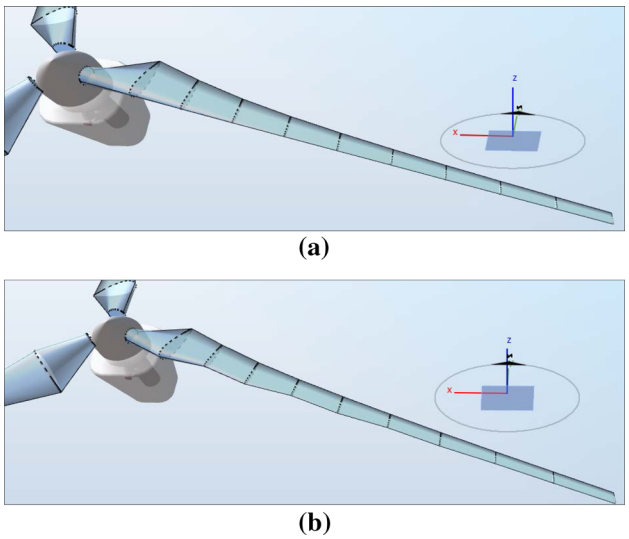

Fig. 28 Blade geometries recreated and visualized in Ashes®. **a** Baseline blade and **b** WLE blade

Lastly, the blade geometries were recreated in Ashes (see Fig. 28). All airfoil shapes were imported as text files after exporting them from the Airfoil Design module in Albatros Create. The geometrical exploration of the blade is not interactive. New blades must be loaded from text files, so the user must determine all geometrical parameters externally. These parameters allow determining the radial distance of an arbitrary number of sections, their chord length, twist angle, relative thickness, and pitch axis distance (similar to Δ_{par}). Based on the summary table in the Albatros Create Dashboard, the text files for recreating the two blade geometries were filled out.

There is a 3D visualizer in Ashes, but it does not allow a real-time inspection of the blade geometry during a geometric exploration. Also, the longitudinal blade transitions are in straight segments. The blades can be exported as STEP files. However, when these files were imported from SOLIDWORKS, no solid bodies or surfaces were detected. With Glovius®, a CAD viewer, it was found that these STEP files contained the information of the 2D curves of the blade sections, but not the aerodynamic surfaces.

8 Conclusions

A generative tool, Albatros Create®, was developed to support an intuitive and accessible geometrical exploration of the aerodynamic surfaces of horizontal-axis wind turbines with or without a Wavy Leading Edge. 3D models can be automatically generated in SOLIDWORKS ®. The modeled features are easily editable, seeking the design process to be seamlessly continued in the CAD software. For an iterative and generative process within the design framework of a turbine, this software should be complemented with additional evaluative tools.

The parameterization was undertaken at the level of the airfoil 2D coordinates, the blade layout, and the rotor. The blade layout consists of a circular root and 10 airfoil sections that can be scaled, displaced, and tilted. These transformations also determine the shape of the Wavy Leading Edge, scaling and displacing forward the sections at the peaks. With a centralized control, these peaks are defined so as to follow a constant, linear, or parabolic trajectory.

Several optimization models based on the blade element momentum theory were included. These models may be used to determine the chord lengths and twist angles for a conventional turbine, or as a baseline for a turbine with Wavy Leading Edge. It was seen that the well-known Betz and Schmitz models tend to converge towards the blade tip. Also, with larger induction factors, the optimum twist angles decrease along the blade. The optimum chord lengths increase with larger axial induction factors and smaller radial induction factors. When the aerodynamic losses due to the induced vorticity and drag are considered, the optimum chord lengths are reduced towards the root and tip. This is more pronounced with larger drag coefficients and with smaller induction factors.

Albatros Create was implemented in the design of a rotor with its baseline layout optimized according to Schmitz. A second version was generated with a Wavy Leading Edge with parabolic control. The 3D models obtained presented surfaces with smooth and continuous curvatures. These geometries were attempted to be recreated in the softwares QBlade, JBLADE, Bladed, and Ashes. It was possible to recreate the scale, inclination, and displacements of the blade sections in the four tools. Nonetheless, JBLADE did not allow defining a circular root, and Bladed did not allow recreating any of the intended airfoil profiles. Although the Wavy Leading Edge was partially introduced in the four tools, there was not a centralized control of its parameters. None of the tools managed to generate surfaces with smooth longitudinal transitions. Also, none produced a CAD model that could be directly edited and used in further design stages. Moreover, the visualization tools of these softwares facilitated a general understanding of the blade geometry but a detailed fine-tuning was challenging.

The generative functionalities of Albatros Create were found to be highly competitive regarding geometric flexibility and control, infographic guidance, and visualization. The capabilities concerning interactive fine-tuning, Wavy Leading Edge, and automatic 3D modeling were unmatched in the benchmarking. Several considerations for following versions of the software include the possibility to add an arbitrary number of blade sections, additional controls for section alignment and the interaction between the Wavy Leading Edge and the baseline geometry, pre-loaded blade templates, a spline tool for freely creating airfoils, and an integration with the XFOIL code to allow 2D aerodynamic analysis. Moreover, the quality of the surfaces produced with Albatros Create will be further evaluated and, if possible, improved.

Acknowledgements The authors would like to thank Santiago Bernal Del Rio, who participated in the development of the GUI and the implementation of the NACA equations in conjunction with Baptiste Simon Lepage, and to Valentin Niclas, who participated in the development of the functionalities programmed in Visual Basic for Applications. Special thanks to Universidad EAFIT through the postgraduate studies grant "Undergraduate research excellence scholarship". Also, special thanks to Colciencias (Colombian Administrative Department of Science, Technology and Innovation) and Universidad EAFIT, who sponsored the "Young Researchers and Innovators Program" in the 645-2014 and 761-2016 calls. This research has been developed in the framework of the Research Program "Estrategia de transformación del sector energético Colombiano en el horizonte de 2030-ENERGETICA 2030", code 58667, funded by the World Bank through Colciencias' 778-2017 call - Scientific Ecosystem, Contract FP44842-210-2018.

References

1. Abbott, I.H., Von Doenhoff, A.E.: Theory of Wing Sections, Including a Summary of Airfoil Data. Courier Corporation, North Chelmsford (1959)
2. Abbott, I.H., Von Doenhoff, A.E., Stivers Jr, L.: Summary of airfoil data (1945)
3. Akour, S.N., Al-Heymari, M., Ahmed, T., Khalil, K.A.: Experimental and theoretical investigation of micro wind turbine for low wind speed regions. Renewab. Energy **116**, 215–223 (2018). https://doi.org/10.1016/j.renene.2017.09.076. http://www.sciencedirect.com/science/article/pii/S0960148117309461
4. Asli, M., Mashhadi Gholamali, B., Mesgarpour Tousi, A.: Numerical analysis of wind turbine airfoil aerodynamic performance with leading edge bump. Math. Probl. Eng. **2015** (2015)

5. Bai, C.J., Lin, Y.Y., Lin, S.Y., Wang, W.C.: Computational fluid dynamics analysis of the vertical axis wind turbine blade with tubercle leading edge. J. Renew. Sustain. Energy **7**(3), 033,124 (2015). https://doi.org/10.1063/1.4922192
6. Bassett, K., Carriveau, R., Ting, D.K.: 3d printed wind turbines part 1: design considerations and rapid manufacture potential. Sustain. Energy Technol. Assess. **11**, 186–193 (2015). https://doi.org/10.1016/j.seta.2015.01.002. http://www.sciencedirect.com/science/article/pii/S221313881500003X
7. Bezrukovs, V.P., Bezrukovs, V.V., Zacepins, A.J.: Comparative efficiency of wind turbines with different heights of rotor hubs: performance evaluation for latvia. J. Phys. Conf. Ser. **524**(1), 012,113 (2014). http://stacks.iop.org/1742-6596/524/i=1/a=012113
8. Blades, E., Miskovish, S., Luke, E., Collins, E., Kurkchubashe, A.: Multiphysics simulation capability using the simulia co-simulation engine. In: 20th AIAA Computational Fluid Dynamics Conference (2011)
9. Bukala, J., Damaziak, K., Kroszczynski, K., Krzeszowiec, M., Malachowski, J.: Investigation of parameters influencing the efficiency of small wind turbines. J. Wind Eng. Ind. Aerodyn. **146**, 29–38 (2015)
10. Burton, T., Jenkins, N., Sharpe, D., Bossanyi, E.: Wind Energy Handbook. Wiley, New York (2011)
11. Čarija, Z., Marušić, E., Novak, Z., Fućak, S.: Numerical analysis of aerodynamic characteristics of a bumped leading edge turbine blade. Eng. Rev. **34**(2), 93–101 (2014)
12. Chen, J., Li, S., Nguyen, V.: The effect of leading edge protuberances on the performance of small aspect ratio foils. In: 15th International Symposium on Flow Visualization, pp. 25–28 (2012)
13. Chou, J.S., Chiu, C.K., Huang, I.K., Chi, K.N.: Failure analysis of wind turbine blade under critical wind loads. Eng. Fail. Anal. **27**, 99–118 (2013)
14. Corsini, A., Delibra, G., Sheard, A.G.: On the role of leading-edge bumps in the control of stall onset in axial fan blades. J. Fluids Eng. **135**(8), 081,104 (2013)
15. Dassault Systemes: Solidworks api help (2018). http://help.solidworks.com/2018/English/api/sldworksapiprogguide/Welcome.htm
16. Dassault Systemes: Solidworks help: Splines (2018). http://help.solidworks.com/2016/english/solidworks/sldworks/c_splines.htm
17. Dassault Systemes: Solidworks help: When to use a boundary (2018). http://help.solidworks.com/2018/english/SolidWorks/sldworks/c_boundary_features.htm
18. Deperrois, A.: Xflr5 analysis of foils and wings operating at low reynolds numbers. Guidelines for XFLR5 (2009)
19. ECN Wind Energy Industrial Support: Blade optimization tool bot user manual (2009). https://www.ecn.nl/publicaties/ECN-E--09-092
20. El khchine, Y., Sriti, M.: Improved blade element momentum theory (bem) for predicting the aerodynamic performances of horizontal axis wind turbine blade (hawt). Tech. Mech. **38**, 191–202 (2018). https://doi.org/10.24352/UB.OVGU-2018-028
21. Favier, J., Pinelli, A., Piomelli, U.: Control of the separated flow around an airfoil using a wavy leading edge inspired by humpback whale flippers. Comptes Rendus Mécanique **340**(1), 107 – 114 (2012). https://doi.org/10.1016/j.crme.2011.11.004. http://www.sciencedirect.com/science/article/pii/S1631072111001902. Biomimetic flow control
22. Fazelpour, F., Soltani, N., Soltani, S., Rosen, M.A.: Assessment of wind energy potential and economics in the north-western iranian cities of tabriz and ardabil. Renew. Sustain. Energy Rev. **45**, 87–99 (2015)
23. Fischer, X., Coutellier, D.: Research in interactive design. In: Proceedings of Virtual Concept 2005. Springer, Paris (2006). https://books.google.com.co/books?id=sjvQx_x_HTQC
24. Fischer, X., Daidié, A., Eynard, B., Paredes, M.: Research in Interactive Design (Vol. 4). Springer, Berlin (2016)
25. Fish, F.E.: Biomimetics: determining engineering opportunities from nature. In: Biomimetics and Bioinspiration, vol. 7401, p. 740109. International Society for Optics and Photonics (2009)
26. Fish, F.E., Howle, L.E., Murray, M.M.: Hydrodynamic flow control in marine mammals. Integr. Comp. Biol. **48**(6), 788–800 (2008)
27. Gasch, R., Twele, J.: Wind Power Plants: Fundamentals, Design, Construction and Operation. Springer, Berlin (2011)
28. Garrad Hassan, G.L.: Bladed educational introductory guide (2014). https://confluence.cornell.edu/display/SIMULATION/Bladed+-+GH+Bladed+Basics
29. Guo, T., Wu, D., Xu, J., Li, S.: The method of large-scale wind turbine blades design based on matlab programming. In: SUPERGEN'09. International Conference on Sustainable Power Generation and Supply, 2009, pp. 1–5. IEEE (2009)
30. Hadi, F.A.: Diagnosis of the best method for wind speed extrapolation. Int. J. Adv. Res. Electr. Electron. Instrum. Eng. **4**(10), 8176–8183 (2015)
31. HFI TU Berlin: Qblade: Wind turbine design and simulation (2014). http://q-blade.org/
32. Huang, G.Y., Shiah, Y., Bai, C.J., Chong, W.: Experimental study of the protuberance effect on the blade performance of a small horizontal axis wind turbine. J. Wind Eng. Ind. Aerodyn. **147**, 202–211 (2015). https://doi.org/10.1016/j.jweia.2015.10.005. http://www.sciencedirect.com/science/article/pii/S0167610515002469
33. Johansen, J., Sørensen, N.N.: Aerodynamic investigation of winglets on wind turbine blades using cfd. Technical ReportRISO (2006)
34. Kundu, P., Cohen, I., Dowling, D.: Fluid Mechanics. Elsevier Science, Amsterdam (2015). https://books.google.com.co/books?id=EehDBAAAQBAJ
35. Ladson, C.L., Brooks Jr, C.W.: Development of a computer program to obtain ordinates for naca 4-digit, 4-digit modified, 5-digit, and 16 series airfoils (1975)
36. Ladson, C.L., Brooks Jr, C.W., Hill, A.S., Sproles, D.W.: Computer program to obtain ordinates for naca airfoils (1996)
37. Lanzotti, A., Carbone, F., Grazioso, S., Renno, F., Staiano, M.: A new interactive design approach for concept selection based on expert opinion. Int. J. Interactive Des. Manuf. (IJIDeM) **12**(4), 1189–1199 (2018). https://doi.org/10.1007/s12008-018-0482-8
38. Mahmuddin, F.: Rotor blade performance analysis with blade element momentum theory. Energy Procedia **105**, 1123–1129 (2017). https://doi.org/10.1016/j.egypro.2017.03.477. http://www.sciencedirect.com/science/article/pii/S1876610217305180. 8th International Conference on Applied Energy, ICAE2016, 8-11 October 2016, Beijing, China
39. Manwell, J.F., McGowan, J.G., Rogers, A.L.: Wind Energy Explained: Theory, Design and Application. Wiley, New York (2010)
40. Marten, D., Wendler, J.: Qblade guidelines. Ver. 0.6, Technical University of (TU Berlin), Berlin, Germany (2013)
41. Marten, D., Wendler, J., Pechlivanoglou, G., Nayeri, C., Paschereit, C.: Qblade: an open source tool for design and simulation of horizontal and vertical axis wind turbines. Int. J. Emerg. Technol. Adv. Eng. **3**(3), 264–269 (2013)
42. Molina, A., Ponce, P., Baltazar Reyes, G.E., Soriano, L.A.: Learning perceptions of smart grid class with laboratory for undergraduate students. Int. J. Interact. Des. Manuf. (IJIDeM) **13**(4), 1423–1439 (2019). https://doi.org/10.1007/s12008-019-00603-5
43. Monteiro, J.P., Silvestre, M.R., Piggott, H., André, J.C.: Wind tunnel testing of a horizontal axis wind turbine rotor and comparison with simulations from two blade element momentum codes. J. Wind Eng. Industrial Aerodyn. **123**, 99 – 106 (2013). https://doi.org/10.1016/j.jweia.2013.09.008. http://www.sciencedirect.com/science/article/pii/S0167610513001967

44. Morgado, J., Silvestre, M., Páscoa, J.: Validation of new formulations for propeller analysis. J. Propul. Power **31**(1), 467–477 (2014)
45. Moriarty, P.J., Hansen, A.C.: Aerodyn theory manual. Tech. rep., National Renewable Energy Lab., Golden, CO (US) (2005)
46. Mortazavi, S.M., Soltani, M.R., Motieyan, H.: A pareto optimal multi-objective optimization for a horizontal axis wind turbine blade airfoil sections utilizing exergy analysis and neural networks. Journal of Wind Engineering and Industrial Aerodynamics **136**, 62–72 (2015). https://doi.org/10.1016/j.jweia.2014.10.009. http://www.sciencedirect.com/science/article/pii/S0167610514002116
47. Nadeau, J.P., Fischer, X.: Research in interactive design. Volume 3, Virtual, interactive and integrated product design and manufacturing for industrial innovation. Springer, Paris (2011)
48. Pennycuick, C.J.: Modelling the Flying Bird, vol. 5. Elsevier, Amsterdam (2008)
49. Planchard, D.C.: Solidworks 2014 reference guide. Tech. rep., SDC publications (2014)
50. Raffaeli, R., Germani, M.: Advanced computer aided technologies for design automation in footwear industry. Int. J. Interact. Des. Manuf. (IJIDeM) **5**(3), 137 (2011)
51. Rafiee, A., der Male, P.V., Dias, E., Scholten, H.: Interactive 3d geodesign tool for multidisciplinary wind turbine planning. J. Environ. Manag. **205**, 107–124 (2018). https://doi.org/10.1016/j.jenvman.2017.09.042. http://www.sciencedirect.com/science/article/pii/S0301479717309118
52. Sedaghat, A., Assad, M.E.H., Gaith, M.: Aerodynamics performance of continuously variable speed horizontal axis wind turbine with optimal blades. Energy **77**, 752–759 (2014)
53. Sedaghat, A., Hassanzadeh, A., Jamali, J., Mostafaeipour, A., Chen, W.H.: Determination of rated wind speed for maximum annual energy production of variable speed wind turbines. Appl. Energy **205**(Supplement C), 781 – 789 (2017). https://doi.org/10.1016/j.apenergy.2017.08.079. http://www.sciencedirect.com/science/article/pii/S0306261917310978
54. Shaviv, E.: Design tools for bio-climatic and passive solar buildings. Solar Energy **67**(4), 189–204 (1999). https://doi.org/10.1016/S0038-092X(00)00067-0. http://www.sciencedirect.com/science/article/pii/S0038092X00000670
55. Silvestre, M.A., Morgado, J.P., Pascoa, J.: Jblade: a propeller design and analysis code. In: 2013 International Powered Lift Conference, p. 4220 (2013)
56. Simis, a spin-off from the Norwegian University of Science and Technology: ashes: Blazing fast wind turbine analysis (2018). https://www.simis.io/
57. Tangler, J.L., Somers, D.M.: Nrel airfoil families for hawts. Tech. rep., National Renewable Energy Lab., Golden, CO (1995)
58. Thomassen, P.E., Bruheim, P.I., Suja, L., Frøyd, L., et al.: A novel tool for fem analysis of offshore wind turbines with innovative visualization techniques. In: The Twenty-Second International Offshore and Polar Engineering Conference. International Society of Offshore and Polar Engineers (2012)
59. Timmer, W.: An overview of naca 6-digit airfoil series characteristics with reference to airfoils for large wind turbine blades. In: 47th AIAA Aerospace Sciences Meeting Including the New Horizons Forum and Aerospace Exposition, p. 268 (2009)
60. Tong, F., Qiao, W., Xu, K., Wang, L., Chen, W., Wang, X.: On the study of wavy leading-edge vanes to achieve low fan interaction noise. J. Sound Vib. **419**, 200–226 (2018). https://doi.org/10.1016/j.jsv.2018.01.017. http://www.sciencedirect.com/science/article/pii/S0022460X18300257
61. Tzivelekis, C.A., Yiotis, L.S., Fountas, N.A., Krimpenis, A.A.: Parametrically automated 3d design and manufacturing for spiral-type free-form models in an interactive cad/cam environment. Int. J. Interact. Des. Manuf. (IJIDeM) **11**(2), 223–232 (2017)
62. Universidad EAFIT: Albatros create (2018). http://www.eafit.edu.co/albatroscreate
63. Vasel-Be-Hagh, A., Archer, C.L.: Wind farm hub height optimization. Appl. Energy **195**(Supplement C), 905 – 921 (2017). https://doi.org/10.1016/j.apenergy.2017.03.089. http://www.sciencedirect.com/science/article/pii/S0306261917303306
64. Vergnano, A., Berselli, G., Pellicciari, M.: Parametric virtual concepts in the early design of mechanical systems: a case study application. Int. J. Interact. Des. Manuf. (IJIDeM) **11**(2), 331–340 (2017). https://doi.org/10.1007/s12008-015-0295-y
65. Yoon, H., Hung, P., Jung, J., Kim, M.: Effect of the wavy leading edge on hydrodynamic characteristics for flow around low aspect ratio wing. Comput. Fluids **49**(1), 276–289 (2011). https://doi.org/10.1016/j.compfluid.2011.06.010. http://www.sciencedirect.com/science/article/pii/S0045793011001988
66. Zhang, R.K., Wu, V.D.J.Z.: Aerodynamic characteristics of wind turbine blades with a sinusoidal leading edge. Wind Energy **15**(3), 407–424 (2012). https://doi.org/10.1002/we.479